NUREG/CR-4556

Heat Transfer From A Rod Bundle Under Natural Circulation Conditions

Prepared by K. P. Hallinan, R. Viskanta

School of Mechanical Engineering
Purdue University

Prepared for
U.S. Nuclear Regulatory
Commission

NUREG/CR-4556

Heat Transfer From A Rod Bundle Under Natural Circulation Conditions

Manuscript Completed: December 1985
Date Published: March 1986

Prepared by
K. P. Hallinan, R. Viskanta

School of Mechanical Engineering
Purdue University
West Lafayette, IN 47907

Prepared for
Division of Accident Evaluation
Office of Nuclear Regulatory Research
U.S. Nuclear Regulatory Commission
Washington, D.C. 20555
Under NRC Grant No. G-04-84-006

SUMMARY

A rectangular natural circulation loop with heat exchangers in the vertical legs was used to obtain heat transfer and fluid friction data from a tube bundle under natural circulation conditions. A 21 rod bundle arranged in a square array with a pitch-to-diameter ratio of 1.33 was used as the test heat exchanger. Deionized water at atmospheric pressure was used as the working fluid in the loop. Natural circulation resulted from the density difference of the fluid within the loop between the two vertical legs of the loop.

Steady-state and transient experiments were performed. Based on the steady-state data obtained, empirical correlations for fluid friction and heat transfer of the circulating fluid flowing through the tube bundle were developed. The pressure drop in the loop was found to depend on the Reynolds number. Friction factor relations for laminar forced flow through tube bundles were found to accurately model fluid friction of the circulating fluid through the test bundle. Empirical correlations for the average Nusselt number were developed for both parallel-flow and counter-flow arrangements of the test heat exchanger. The placement of grid spacers on the test bundle was found to have little effect on the total flow resistance of the circulating fluid, while enhancing the average heat transfer from 5% to 15%, depending on the thermal and flow conditions.

The dynamic response of the circulating fluid and of the loop structural components was predicted from a one-dimensional model. The model equations were solved numerically using a finite-difference method. Local temperatures and flow rates of the circulating fluid were predicted for three step changes in the heating rate (start-up, step increase and step decrease). Good correspondence was obtained between the predicted and measured local temperatures and the time to reach steady-state conditions.

ACKNOWLEDGEMENTS

The financial support by the U.S. Nuclear Regulatory Commission Contract No. NRC 84006 is gratefully acknowledged. The authors also wish to express their appreciation to Mr. Jose Reyes for his interest and overall guidance during the performance of this work. The initial support of the work by Argonne National Laboratory under Contract No. 31-109-38-6959 and interest by Dr. P.A. Lottes is acknowledged with thanks.

CONTENTS

LIST OF TABLES

LIST OF FIGURES

NOMENCLATURE

a	Coefficient in Fanning friction factor relation
A_f	Cross-sectional flow area of loop components
A_t	Cross-sectional area of glass tubing
A_{ins}	Cross-sectional area of insulation
b	Constant in Faning friction factor relation
C_I	Constant in expression for Nusselt number on inside of tubes, Eq.(4.14)
C_R	Constant in total resistance relation, Eq. (3.10)
c_p	Specific heat
d_w	diameter of heat exchanger tubes
D_h	Hydraulic diameter defined in Eq. (3.6)
D_t	Inside diameter of glass tubing
f	friction factor
G	Mass flow rate of circulating fluid
Gr	Grashof number defined by Eq.(3.16)

Gr_{m} Grashof number based on average heat flux in the source leg defined by Eq.(3.15)

g Gravitational constant, 9.81 m/s^2

$\bar{h}$ Average heat transfer coefficient on outside of tubes

$\bar{h}_{a}$ Average heat transfer coefficient on outside of insulation in ambient

h_{i} Local heat transfer coefficient on inside of tubes

h_{o} Local heat transfer coefficient of outside of tubes

h_{ot} Local heat transfer coefficient of inside of glass tubing

K_{T} Total form loss coefficient for flow around the loop, see Eq. (3.10)

k Thermal conductivity

L Length of tube bundle in source leg

$\dot{m}$ Mass flow rate of fluid passing through tube bundles

$\overline{Nu}$ Average Nusselt number on outside of tubes

n Number of tubes in a bundle

P Pressure of circulating fluid or perimeter

p Pitch (spacing) of tubes in bundle

P_{ht} Heat transfer perimeter, $(n \times d_{o})$

P_{sh}	Shear perimeter, $(P_{ht} + 2\pi D_g)$
Pr	Prandtl number
p_i	Inside perimenter of tubes
p_o	Outside perimeter of tubes
p_{ot}	Inside perimeter of glass tubing
q	Heat flux
R	Effective flow resistance
s	spatial co-ordinate about the loop
T_f	Local temperature of circulatig fluid in loop
ΔT_D	Driving temperature difference
ΔT_{w-L}	Average temperature difference between tubes and circulating fluid
T_t	Local glass wall temperatures
T_{ins}	Local insulation temperature
T_i	Local temperatures of fluid passing through tube bundles
T_{si}	Local temperature of circulating fluid in source sink leg
T_{so}	Local temperature of circulating fluid in source leg
T_w	Local tube wall temperatures

T_o	Reference temperature of circulating fluid
t	Time
u	Cross-section averaged velocity of circulating fluid
U_{ot}	overall heat transfer coefficient between circulating fluid and ambient
x	Spatial co-ordinate in vertical direction
α	Reciprocal of the flow area integrated about the loop, $\alpha = \int ds/A_f$
β	Thermal coefficient of expansion of water
ε	Porosity of tube bundle
ρ	Density of fluid or loop structural components
τ_w	Frictional wall shear stress
μ	Dynamic viscosity of fluid.

1. INTRODUCTION

1.1 Background

Natural circulation loops (thermosyphons), created by heat addition and removal to/from a fluid in different parts of the system, arise in many engineering applications, including some cooling modes of nuclear reactors, computer cooling applications, solar heating and cooling systems, geothermal power production, and process industry. In the loop, there is fluid flow due to buoyant forces that result from the density difference between the heated and cooled parts of the loop.

General reviews of thermosyphons including applications have been given (Japikse, 1973; McKee, 1979; Norton and Probert, 1982; Zvirin, 1981; Mertol and Greif, 1984). One of the major uses of natural circulation loops arises in some cooling modes of nuclear reactor applications. The problem of decay heat removal from the core by natural convection circulation has gained interest, particularly after the Three Mile Island (TMI) accident. Reviews specifically concerned with nuclear reactor applications of natural circulation loops have been prepared (Zvirin, 1981; Zvirin and Rabinoviz, 1983). Thermosyphons may become unstable under certain conditions and have been recently reviewed (Mertol and Greif 1984). Unstable flows are of concern in asymmetric flow situations where heat removal is necessary, such as in nuclear reactor cooling. They can lead to flow stagnation and flow reversals, causing local temperature increases. In extreme situations boiling may occur, followed by core uncovering and damage to the fuel rods.

Often, in natural circulation loops, tube or rod bundles are used to provide the source of heat addition and the sink for heat removal. However, a literature review following the TMI-2 nuclear reactor accident revealed an availability of basic heat transfer and fluid friction data for natural circulation flow axial to the tubes (Viskanta and Mohanty, 1981). Gruszczynski and Viskanta (1983) have performed experiments using a bundle with a triangular tube array as the source of heat in a vertical leg of a closed rectangular loop. They developed empirical correlations for the average Nusselt number and friction factor applicable to loops of similar geometry. No other known work appears to provide such useful correlations for natural convection circulation in tube bundles. Zvirin et al., however, did calculate the pressure drop about a loop, typical of pressurized water reactors (PWR's) (Zvirin et al. 1981).

The very limited results for natural circulation flows are meaningful only for the geometry used and the type of heat input (i.e., constant temperature, constant heat flux, etc.). No general conclusions can be drawn from the preceding work to apply toward natural circulation loops of different geometries and heat inputs. Therefore, forced flow results, which are documented for

a wide range of geometries, are used to provide comparisons with natural circulation results. It has been determined, in general, that friction factors and heat transfer coefficients for natural circulation flows are higher than would be predicted from forced flow correlations (Gruszczynski and Viskanta, 1983). For example, Kemeney and Somers (1981) have shown that as natural convection effects become more significant in combined free and forced convection flow in vertical tubes, the friction factor, based on the Reynolds number, increases above the value that would be predicted by the forced flow relation. An analysis of combined convection heat transfer in an infinite rod array by Yang (1979) with uniform imposed heat flux indicates that the effect of natural convection is to increase the Nusselt number and pressure drop.

Some important results from axial forced convection flows over tube bundles should still be applicable to natural circulation flows. Sparrow and Loeffler (1959) have presented an analytical solution for longitudinal, fully developed laminar flow between cylinders to determine pressure drop and friction factors for arrays with different porosities. They found that the friction factor increases as the porosity of the bundle decreases. For laminar forced flow, Schmid (1966) has shown that, except for small pitch-to-diameter ratios, each individual tube could be considered isolated from the other tubes. The tube bundle could then be divided into a number of cells. All correlations would be based on this "effective flow area about one tube. Mohanty and Roy (1979) have found that the experimental data for the friction factor in laminar flow could accurately be correlated with Blasius correlations using the hydraulic diameter of one tube based on the effective flow area. Up-to-date reviews of fluid friction and heat transfer data for low Reynolds number, forced convection flow are available (Johansen, 1983a, Johansen, 1983b, Rehme, 1983) and there is no need to repeat them here.

Grid spacers are often used to separate rods in PWR fuel assemblies. Much work has been done to determine their effect on heat transfer and pressure drop for forced flow conditions. No work appears to have been reported, however, considering these effects in natural circulation flows. Based on previous results (Johansen, 1983a; Vieck and Weber, 1970; Marek and Rehme, 1979; Bragina et al., 1981) it has been determined that the blockage in the flow created by the grid spacers increases the pressure drop and enhances the heat transfer due to mixing in the region of the spacer. The enhanced heat transfer is maximum in the vicinity of the spacer grid and diminishes exponentially downstream of the spacer. Yao et al. (1982) have presented the most comprehensive collection of the existing pressure drop and heat transfer data. They also have reported an empirical relation correlating the data for the different geometries considered.

1.2 Objectives and Scope of Research

The main objective of this research is to gain a better understanding of fluid flow and heat transfer of a single-phase fluid for natural circulation flow longitudinal to a tube bundle which is prototypic of PWR fuel elements. The specific goals of the research project are the following:

1. Measure heat transfer coefficients on a tube bundle in the absence of rod spacers under natural circulation conditions in an atmospheric pressure loop using water as a working fluid and correlate the experimental data.

2. Measure heat transfer coefficients on a bundle with rod spacers and correlate the experimental data.

3. Develop a model to predict the dynamic behavior of the natural convection circulation loop (circulation fluid and structural components) and compare the results with the experimental data.

2. EXPERIMENTS

2.1 Natural Circulation Loop and Tube Bundles

The single-phase natural circulation loop used in the experiments is shown schematically in Fig.2.1. The loop is constructed from Kimax glass tubing and consists of a tube bundle (i.e., heat exchangers) in each of the two vertical legs of a rectangular loop. The inside diameter of the glass tubing is 7.62 cm. To insure that the manufacturer's specification for the safe pressure of the glass loop is not exceeded during operation, a reservoir is fitted to one of the top flanges, open to the atmosphere. This feature allows for normal operation of the loop at atmospheric pressure. The loop is insulated with three layers of 2.54 cm thick Johns-Manville insulation tubing on the vertical and horizontal legs as well as on each of the tees.

The two tube bundles shown in Fig.2.1 provide a means for heat addition and removal using water as the working fluid. The tube bundle (#1) in the hot leg serves as the heat source in the natural circulation loop, whereas the other tube bundle (#2) in the cold leg serves as the heat sink. The inlets and outlets to each of the tube bundles could be interchanged to allow both counter-flow and parallel-flow heat exchange. Dimensions and characteristics of each tube bundle are given in Table 2.1 and Fig.2.2.

Tube bundle #1 was constructed of a cluster of twenty-one copper tubes arranged in a rectangular array, having a pitch-to-diameter ratio (PDR) of 1.33. Tube bundle #2 was constructed of seven copper tubes arranged in a triangular array with a PDR of 1.25. The arrangement shown for tube bundle #1 was chosen because the array is similar in geometry to PWR fuel elements.

Heating and cooling fluid was supplied by cold and hot water lines along with a high pressure steam line. The cooling fluid was supplied by a cold water line at a temperature of $14 \pm 2^{\circ}$C.

2.2 Instrumentation

The loop was instrumented so that the heat addition to the loop could be determined from the measured temperature changes across, and the mass flow rates of the working fluid through the tube bundles. Because of the low velocities of the circulating fluid in the loop, invasive methods could not be used for the measurement of the local velocity without disturbing the flow field. Optical methods such as LDV (Morrison and Ranatunga 1980) could be used for such a purpose, but the technique is also fraught with difficulties such as the precise location of the test volume in a fluid which has large temperature gradients and a rather strong variation of the index of refraction with temperature. The velocity of the fluid in a natural circulation

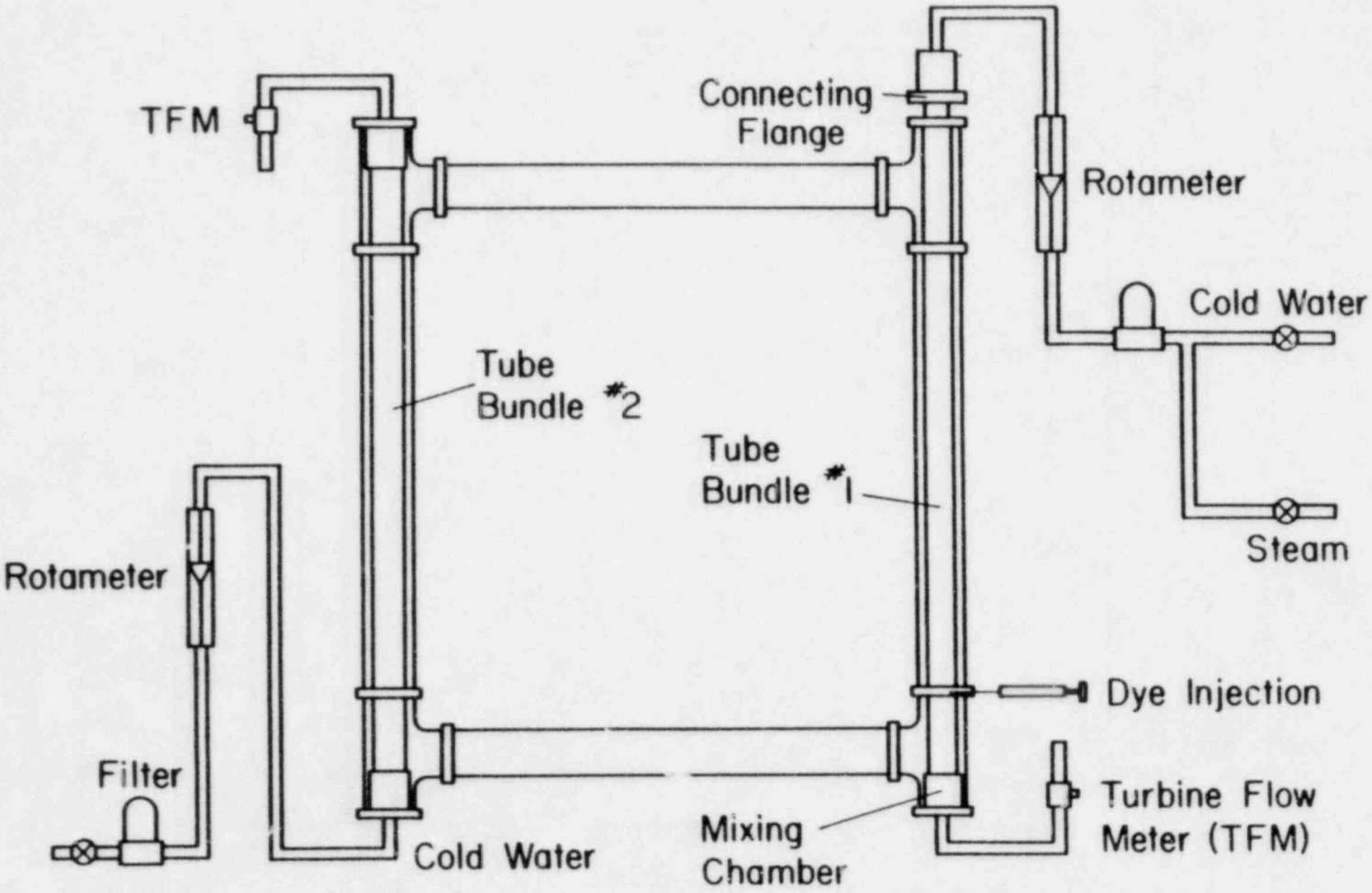

Figure 2.1 Schematic diagram of the experimental loop.

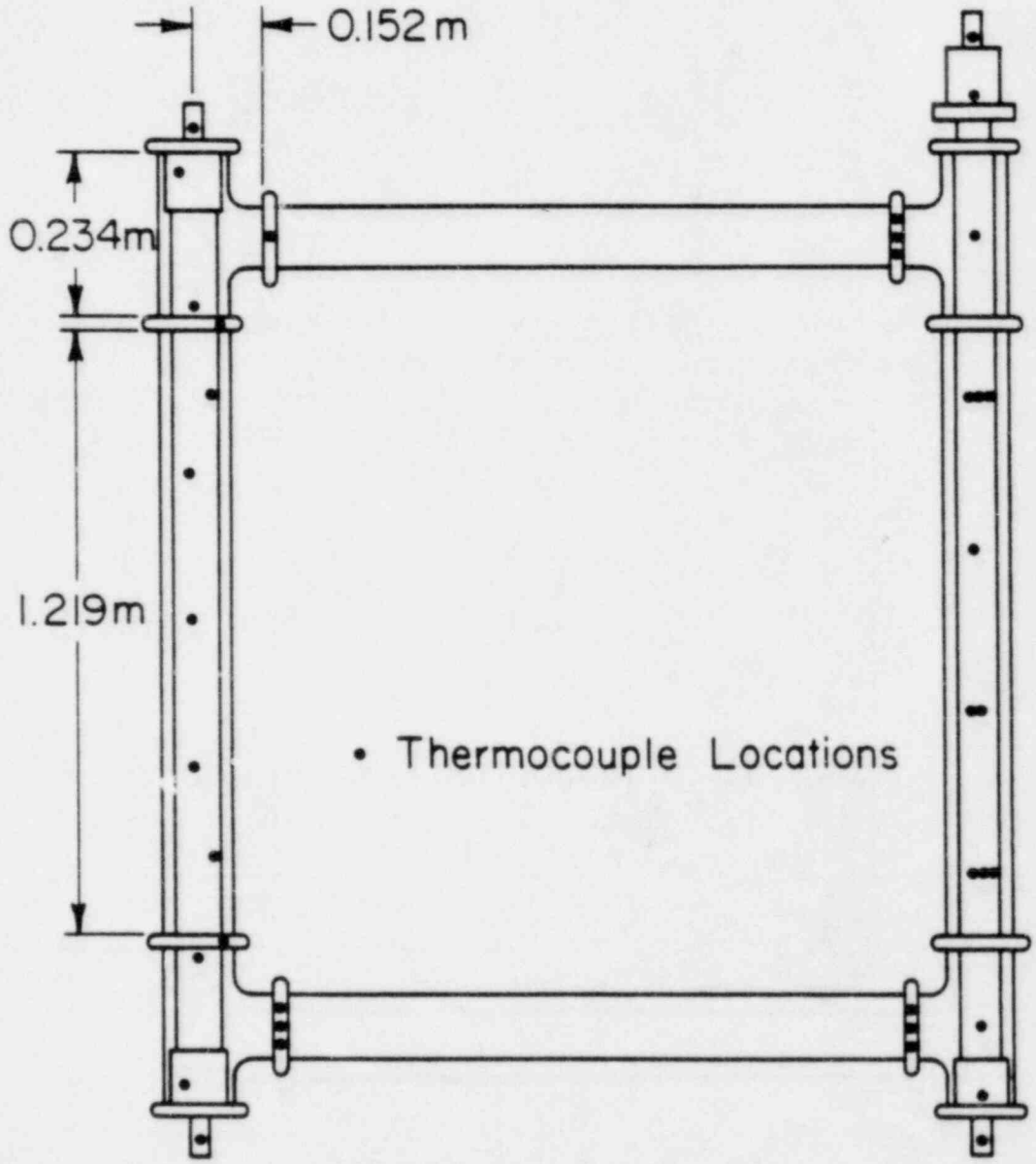

Figure 2.2 Loop dimensions and thermocouple positions.

Table 2.1. Dimensions and characteristics of the tube bundles and loop

Dimensions	Tube Bundle #1	Tube Bundle #2
No. of tubes	21	7
OD of tubes (mm)	9.55	19.05
Tube thickness (mm)	1.587	1.02
Length of tube bundle (m)	1.6515	1.575
Cross-sectional flow area (m^2)	0.003064	0.002565
Type of array	Rectangular	Triangular
Pitch to diameter ratio	1.33	1.25
Hydraulic diameter (m) (heat transfer)	0.0195	0.0245
Hydraulic diameter (m) (shear area)	0.0141	0.0156
Hydraulic diameter (m) (equiv. flow area)	0.012	0.0138
Length of horizontal legs of loop (m)	1.486	1.486
Length of vertical legs of loop (m)	1.499	1.499
Total volume of water in loop (m^3)	0.2145	0.2145
Porosity (area of bundle/area of loop leg)	0.67	0.57

loop could also be determined using dye-traicing (Ong, 1974), but in a tube bundle the dye rapidly looses contrast because of diffusion and secondary flow. Therefore, the mass flow rate of the circulating fluid in the loop was determined indirectly from an energy balance on the loop and the tube bundles at steady-state conditions only.

The loop was instrumented with copper-constantan thermocouples. On tube bundle #1, six equally spaced thermocouples were placed along the outside wall of the central tube to measure the wall temperature along this tube. Three thermocouples were placed

along the outside wall of the central tube to measure the wall temperature along this tube. Three thermocouples were placed along the outside wall of a tube adjacent to the central tube, and two thermocouples were placed along the outside wall of one of the outer tubes. The off-center tubes were instrumented to determine if any differences in wall temperature between the central and outer tubes were evident. Similarly, seven thermocouples were soldered to tube bundle #2, five along the central tube and two on one of the outer tubes.

In addition to these thermocouples, a differential thermocouple was set up across each tube bundle to accurately measure the temperature difference of the heating/cooling fluid across the tube bundles. Also, in each header of both tube bundles (Fig.2.3), copper-constantan thermocouples were installed to directly measure the mixed-mean temperature of the fluid at the inlets and outlets of the heat exchangers. Special mixing chambers were designed and installed in the two tube bundles for insuring that true mixing-cup temperatures were measured in determining heat addition and removal from the loop.

Thermocouples were installed on both ends of each of the horizontal connecting legs (see Fig.2.2) to measure the mean temperatures of the circulating fluid in the loop at each cross-section. A movable thermocouple probe was used to confirm that the three fixed thermocouples installed in the horizontal legs at the top and bottom of the hot leg indicated the mixed-mean circulating fluid temperature. For all conditions this was within the accuracy of the thermocouples and the data acquisition system. The wall temperatures of the loop tubing were measured by installing many thermocoupes along the outer wall of the tubing at various locations around the loop (Fig.2.2). A total of 42 thermocouples were installed around the loop. The temperature readings were recorded at frequent time intervals using a precalibrated Esterline Angus data logger.

The average heating and cooling fluid flow rates were monitored using Brooks turbine flow meters which were calibrated prior to the tests. The turbine flow meters produce a number of pulses proportional to the flow rate. The pulses were recorded by two Anadex digital counters.

2.3 Flow Visualization

In order to establish the flow regimes of water in the loop, a flange connecting the lower tee to the vertical leg of the glass loop on the side of the heat source was modified to allow for dye injection with a syringe. Previous flow visualization studies in the loop were largely ineffective because the dye was injected in the horizontal connecting legs and became completely mixed with the circulating water in the tees connecting the horizontal to

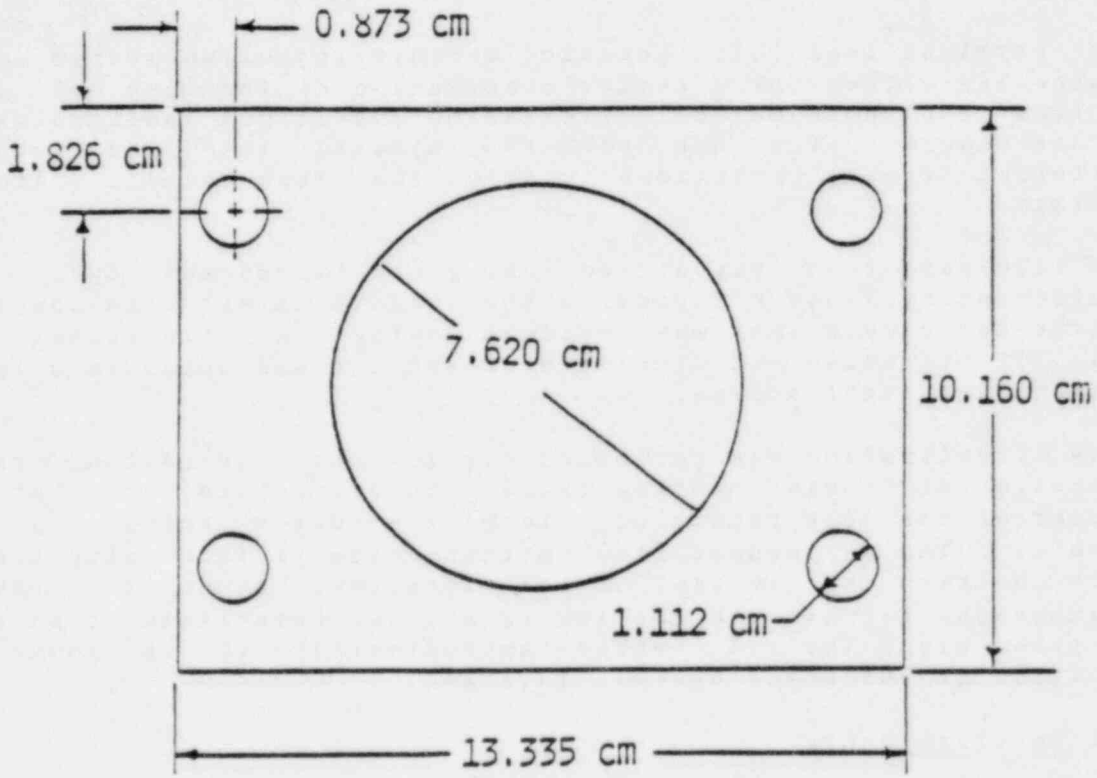

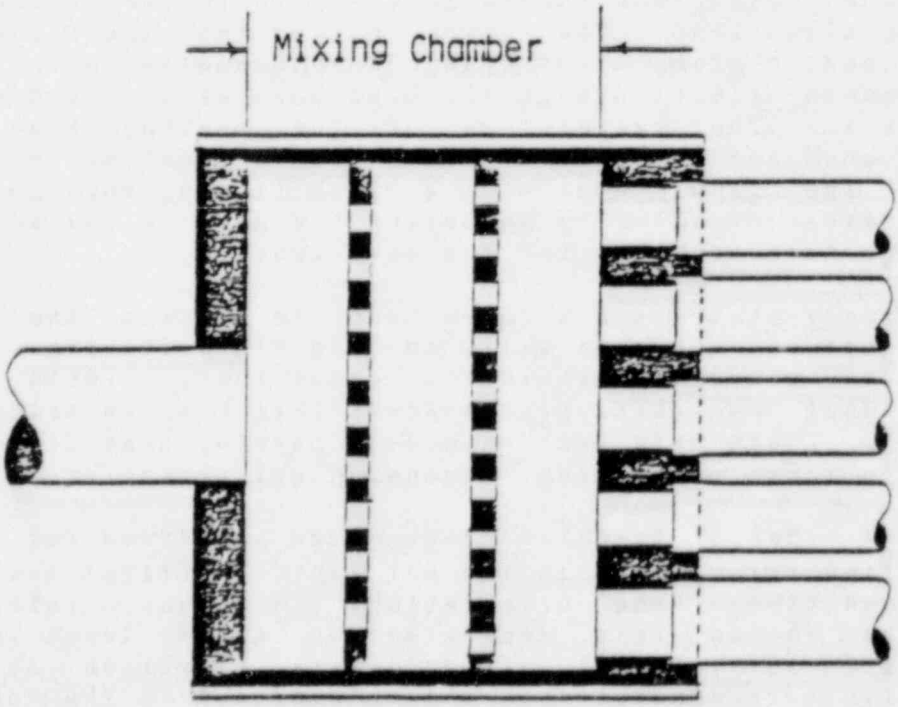

Figure 2.3 Separator plate and mixing chamber.

the vertical legs [8]. Locating the dye injection system on the source leg allows for a better observation of the flow of water in the loop under natural circulation conditions longitudinal to a tube bundle. The dye can be injected into the loop at different radial positions within the tube bundle using a syringe.

The flow was best visualized using a florescent dye. Non-florescent dyes did not provide the sharp contrast with the tubes in the rod bundle that was evident using the florescent dye. Best illumination of the florescent dye was obtained using an ultraviolet light source.

Flow visualization was performed for low and high heating rates. At each of these heating rates, the dye was injected into the center of the tube bundle or along the outer fringes of the bundle. The subsequent flow patterns made visible using the dye were observed at several axial locations along the bundle. Photographs for all the heating rate cases were taken at an axial position along the rod bundle approximately 10 cm above the location at which the dye was injected.

2.4 Test Procedure

The loop was filled with deionized water through the reservoir, located on the top of the cold leg. The copper tube bundle in the hot leg was connected to the heating fluid line described previously. The copper tube bundle in the cold leg was connected to the cooling fluid line. The valves controlling the flow in the cooling and heating lines were opened manually to initiate flow of the working fluid through the tube bundles in the hot and the cold legs. The temperature of the heating line was controlled by changing the rate at which steam was mixed with cold water. The flow rates of the fluid flowing through both tube bundles were controlled by adjusting the gate valves in both lines, and were held constant for the test runs.

A series of steady-state tests were run to obtain the heat transfer data between the tube walls and the fluid flowing within the loop under natural circulation conditions. Tests were performed without and with grid spacers (Fig.2.4) installed on tube bundle #1. These data were needed to develop heat transfer correlations in terms of relevant dimensionless parameters.

Three different types of transient tests were performed for each tube bundle flow arrangement in the hot leg. The first test was a startup condition. The circulating fluid was initially stagnant. The second test consisted of a step input in the heating rate from an initially steady-state operation of the loop. The third test consisted of a step decrease in the heating rate from an initially steady-state operation of the loop. Readings were recorded frequently until steady-state conditions were reestablished in the loop.

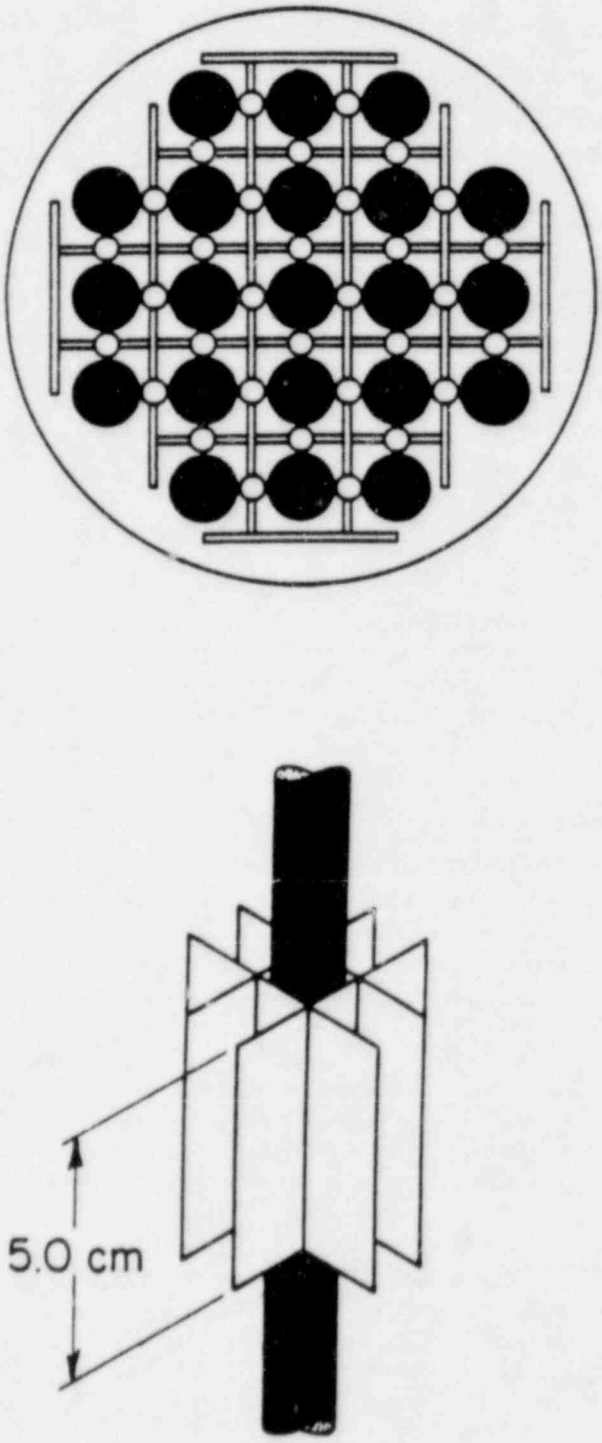

Figure 2.4 Egg-crate type spacer grids.

3. HEAT TRANSFER UNDER STEADY-STATE NATURAL CIRCULATION CONDITIONS

3.1 Steady-State Thermal Analysis of the System

3.1.1 Physical Model and Assumptions

When the hot and cold vertical legs of a natural circulation loop are connected as in Fig. 3.1, the flow in one communicates with the other. A pumping action due to the difference in the average density in the two average legs is present. This is the forced convection component. In other words, the phenomenon in the loop is forced convective, but locally in each of the vertical legs natural convection supports or opposes forced convection. Forced convection cannot occur if the two vertical legs are not connected, irrespective of the heat addition or removal.

A mathematical model has been developed to predict the thermal performance of a single phase natural circulation loop shown in Fig.2.1. A one-dimensional model, where the only space coordinate, s, runs along the components of the loop is adopted to describe the spatial dependence of the mass flow rate and temperature (Zvirin, 1981; Zvirin and Rabinoviz, 1983). The temperature is, then, the cross-sectional average in each component of the loop.

To describe mathematically the thermal performance of a natural circulation loop, we apply the conservation of mass, momentum and energy principles to a differential volume element of fluid or structural component. In the framework of the one-dimensional model, the only spatial coordinate s, runs counterclockwise around the loop. The Boussinesq approximation is adopted, i.e., the density of the fluid is considered constant in the governing equations except in the buoyancy term. The other fluid properties are assumed constant, which is justifiable for the small temperature variations expected. Separate energy balances are made on the working fluid, the tube bundle, the circulating fluid, the loop piping, and the insulation. Axial heat conduction (in the s-direction) along the internal structural components comprising the loop as well as the circulating fluid are neglected in comparison to advection or convection. Kinetic and potential energy changes of the circulating fluid are negligible in comparison to advection and neglected.

3.1.2 Mathematical Model

Under steady-state conditions, and assuming that the circulating flow is incompressible, from the equation of mass conservation, it is apparent that the mass flow rate of the circulating fluid is constant.

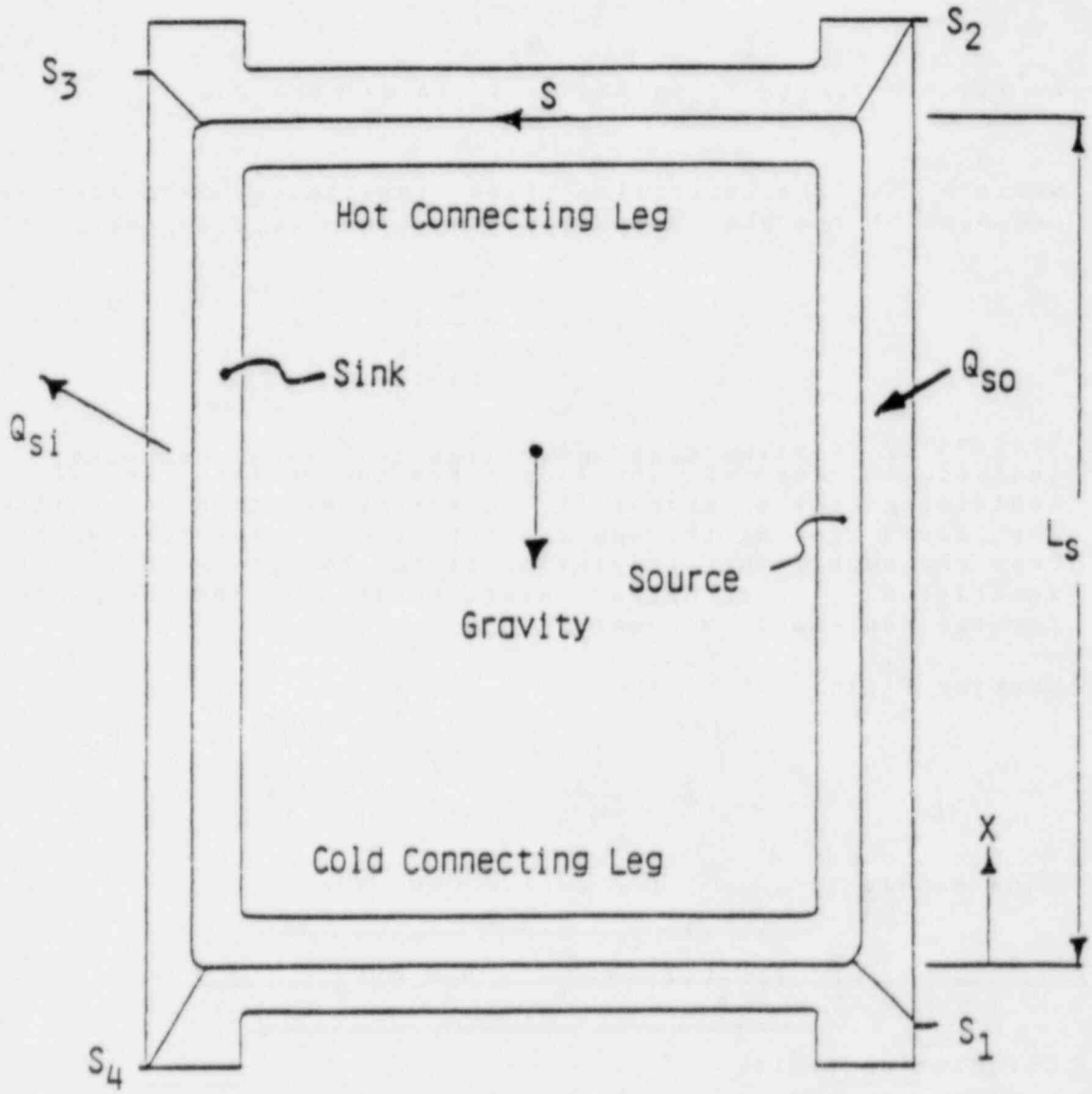

Figure 3.1 Loop coordinates used in the analysis.

Following the analysis of Zvirin et al. (1981), the momentum equations for each leg of the loop were integrated over their respective lengths. This yielding the momentum equation for the entire loop,

$$RG^2/2\rho = \rho_o g\beta L_s\left[\int_0^{L_s} T_{so}(s)dx - \int_0^{L_s} T_{si}(s)dx\right] = \rho_o g\beta L_s \Delta T_D \qquad (3.1)$$

where R is the effective flow resistance parameter and is composed of the sum of the frictional and form losses,

$$R = \sum_i f_i \frac{L_i}{D_{hi}A_i^2} + \sum_j \frac{K_j}{A_j^2} \qquad (3.2)$$

The energy equation must be written for each component of the individual legs of the loop. For the vertical leg of the loop containing heat exchanger #1, an energy equation was written for the fluid flowing through the tube bundle, the tube walls of the heat exchanger, the circulating fluid, the glass walls, and the insulation. Under steady state conditions the energy equations for the components become:

Working Fluid

$$mc_p \frac{dT_i}{ds} = h_i P_i n(T_w - T_i) \qquad (3.3)$$

Tube Bundle

$$h_i P_i n(T_i - T_w) - h_o P_o n(T_w - T_f) = 0 \qquad (3.4)$$

Circulating Fluid

$$Gc_p \frac{dT_f}{ds} = h_o P_o n(T_w - T_f) - U_{ot} P_{ot}(T_f - T_a) \qquad (3.5)$$

The heat transfer rate to the circulating fluid is determined from Eq.(3.3) from the knowledge of the temperature difference and the mass flow rate of the water flowing through the heat exchangers. The mass flow rate of the circulating fluid is determined by equating the heat capacity rates of the fluid flowing through the test bundle and the fluid passing axially over the bundle.

Local temperatures of the fluid flowing through the heat exchangers were calculated knowing the inlet and outlet temperatures for turbulent, hydrodynamically fully developed, thermally developing flow (Grober et al., 1961), and then adjusting a constant in a correlation for the convection heat transfer coefficient h_i so that a numerical solution of Eq.(3.3) results in a calculated outlet temperature equaling the measured one.

Local heat transfer rates were calculated from the knowledge of the local heat transfer coefficients inside the tubes, the "corrected local temperatures" for the fluid flowing through the tubes, and the local tube wall temperatures.

An iterative procedure was used to determine both the local temperatures and local heat transfer coefficients for the circulating fluid. Initially, local temperatures for the circulating fluid in the source leg were assumed. Local values for the heat transfer coefficient on the outside of the tubes could then be determined from Eq.(3.4) then, from Eq.(3.5) new values for the working fluid temperatures were determined based on the calculated values for the local heat transfer coefficients. This procedure was repeated until all of the local temperatures and heat transfer coefficients converged.

The hydraulic diameter used in the above development was defined as

$$D_h = 4A/P_{ht} \quad \text{or} \quad D_h = 4A/P_{sh} \tag{3.6}$$

The perimeter for shear and heat transfer, P_{sh}, and the perimeter for heat transfer P_{ht}, are defined as

$$P_{sh} = n\pi d_w + \pi D_t \tag{3.7}$$

and

$$P_{ht} = n\pi d_w \tag{3.8}$$

For the tube bundles in each of the vertical legs, the hydraulic diameter is typically based on the equivalent flow area around one tube (Sparrow and Loeffler, 1959; Schmid, 1966). In a square array bundle, this flow area is

$$A = S^2 - \pi d_w^2/4 \tag{3.9}$$

where S is the pitch or spacing of the tubes in the bundle. The

perimeter for heat transfer is simply the outer perimeter of one tube, assuming that heat transfer does not vary from tube to tube in the bundle.

3.2 Steady-State Tests in Absence of Grid Spacers

The effect of heat exchanger flow arrangement, heat exchanger flow rates, and heating and cooling rates on heat transfer and fluid friction for longitudinal natural circulation flow through a tube bundle was determined. Listed in Table 3.1 are the conditions for each of the tests.

Table 3.1. Summary of steady-state tests

Data Set	m (kg/s) of Fluid		Heat Exchanger #1
	Cooling	Heating	Arrangement
A	0.050	0.15	Counter-flow
B	0.050	0.09	Counter-flow
C	0.090	0.15	Counter-flow
D	0.050	0.15	Parallel-flow
E	0.050	0.09	Parallel-flow
F	0.090	0.15	Parallel-flow

3.2.1 Flow Visualization and Fluid Friction

The flow was observed to be stable in all cases. Also, the circulating fluid flow rate was observed to almost instantaneously (within 5 seconds) increase/decrease after a step increase/decrease in the heating rate was implemented.

Flow visualization experiments showed a definite transition region from laminar to turbulent flow. On the average, the transition from laminar turbulent flow occurred when

$$Gr = 6.6 \times 10^5 \quad , \quad Gr_m = 4.8 \times 10^5 \quad , \quad Re = 340$$

Figure 3.2 illustrates the relationship between the Reynolds number (Re) and the Grashof number (Gr_{T_D}) for the counter-flow and parallel-flow arrangements. The data were plotted using two different abscissa scales in order to avoid overlap and more clearly present the different results for counter-flow and parallel-flow heating arrangements. Note that the Reynolds number is proportional to the mass flow rate of the circulating fluid in the loop, and the Grashof number, based on the driving temperature difference ΔT_D, is proportional to the heat addition to the system. The results show that for identical heat addition

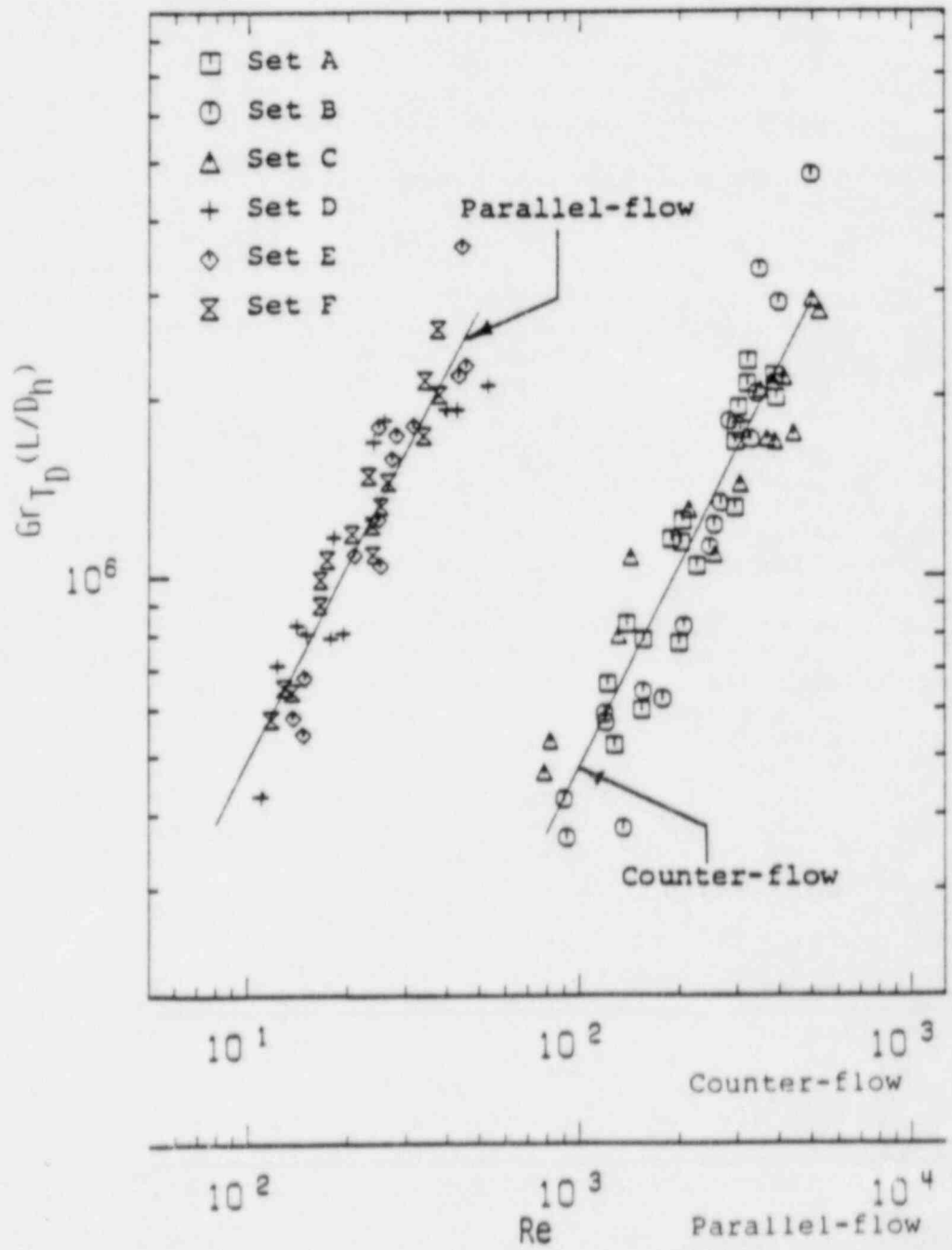

Figure 3.2 Dependence of the Grashof number (based on driving temperature difference) on Reynolds number.

rates the mass flow rate of the circulating fluid in the parallel-flow arrangement is greater than for the counter-flow case. The explanation for this observation is that for parallel-flow a larger temperature difference between the heat exchanger fluid and the circulating fluid at the bottom of the source leg was measured than for the counter-flow case. This resulted in a larger buoyancy driving force, causing a higher mass flow rate of the circulating fluid.

Frictional pressure drop could not be determined experimentally using invasive methods, because the velocity of the circulating fluid was too small. Therefore, the frictional resistances in each of the component legs of the loop was determined indirectly. The analysis of the effective flow resistance parameter R indicates that a plot of RA_f^2 versus 1/Re would be a straight line of the form (Gruszczynski and Viskanta, 1983)

$$RA_f^2 = C_R/Re + K_T A_f^2 \qquad (3.10)$$

where A_f is the cross sectional flow area and Re is the Reynolds number of the circulating fluid in the source leg. The constant C_R is composed of the individual friction factors for each loop component, and K_T is the total form loss coefficient for flow in the loop. Analysis of the data gives a slope of C_R = 8,050 and $K_T A_f^2$ = 1.467 (Fig.3.3). The intercept is nearly zero, indicating that the effect of form losses in the loop is negligible in comparison to the frictional losses.

From this value for C_R, the friction factor relations for the individual legs of the loop can be found. Assuming that in each of the legs the friction factor, f = a/Re, and taking the coefficients a_L = 43 for the horizontal connecting legs and assuming that $a_1 = a_2$ since the porosities of the two bundles are approximately equal, then $a_1 = a_2$ = 31.2. For forced convection laminar flow in a a tube bundle with a squarely arranged 19 tubes and a S/D = 1.3 (approximately the same as the rod bundle used in this study) a_1 was found to be 27 (Mohanty and Roy, 1979).

To better understand the flow and heat transfer regimes under natural circulation conditions, a plot of Re vs. $GrPr(D_h/L)$ was made and is shown in Fig.3.4. The various regimes of flow based on a correlation of these parameters for flow in a vertical pipe are described in the literature (Metais and Eckert, 1964) . Using hydraulic diameters in place of the tube diameters in both the Reynolds and Grashof numbers, the flow in the natural circulation loop is seen to fall within the mixed convection regime.

Mixed convection does in fact exist. Consider a packet of fluid, initially in the source leg as was used by Welander (1967) to describe flow instabilities. Buoyancy differences between the

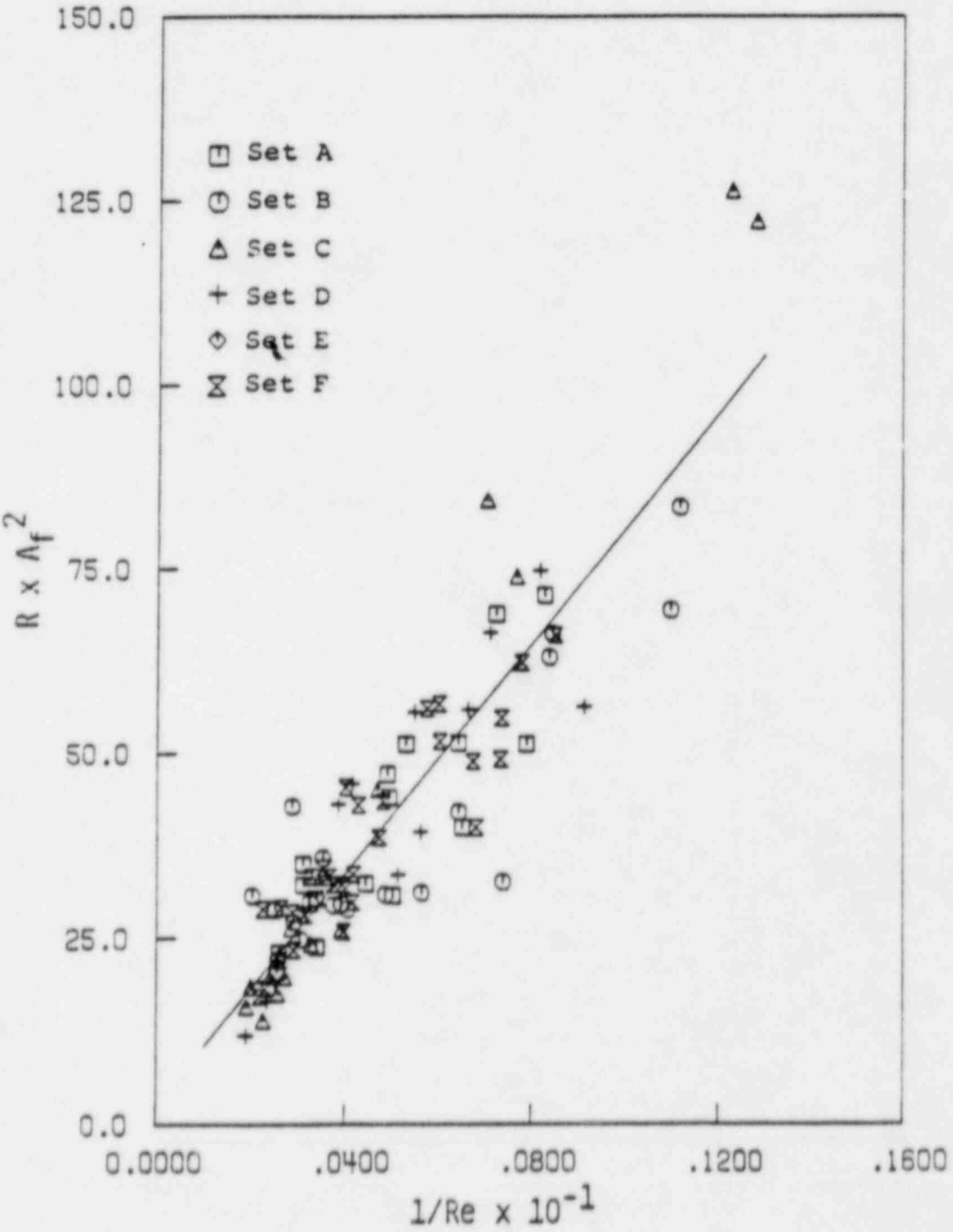

Figure 3.3 Dependence of the effective flow resistance parameter on Reynolds number.

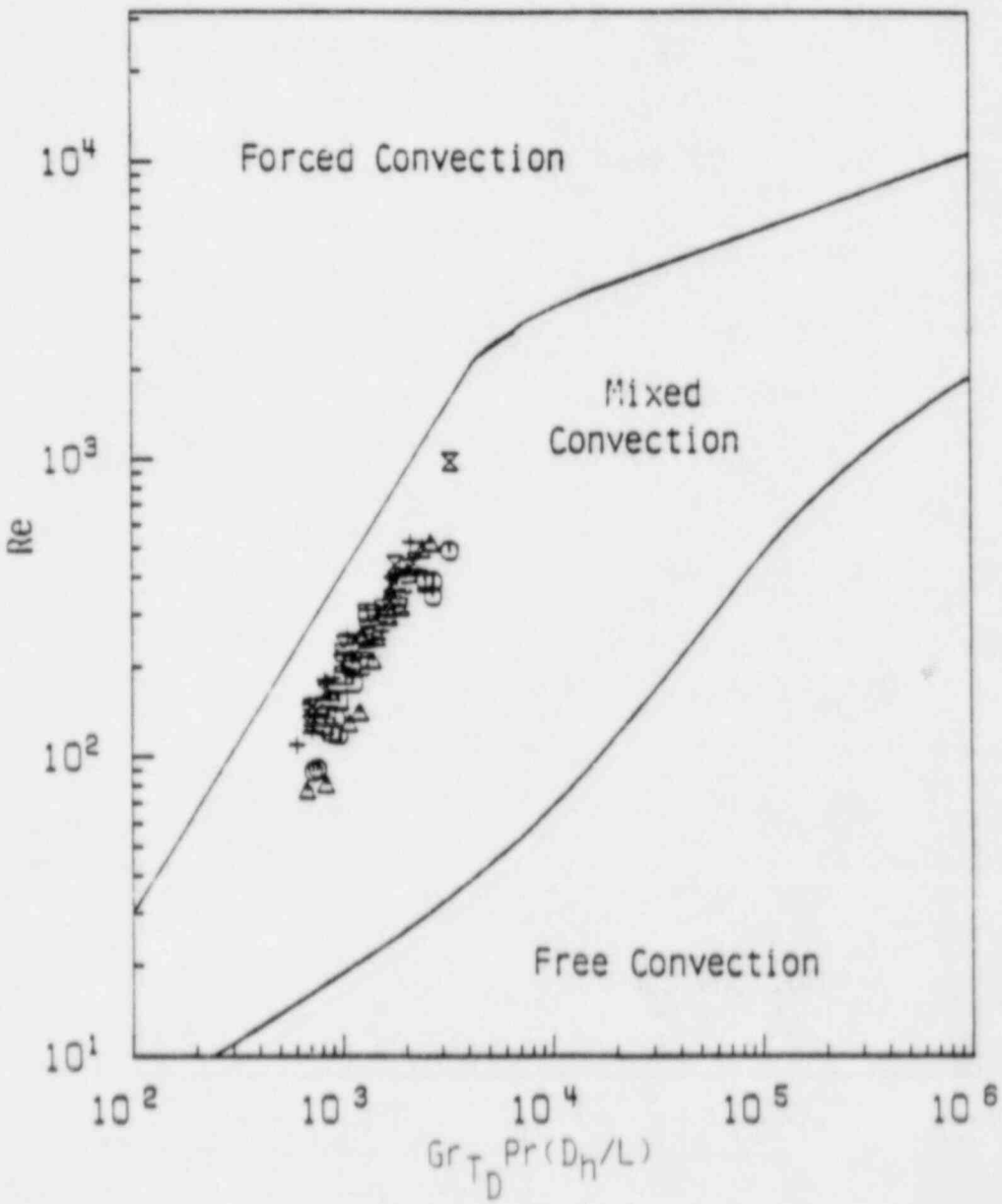

Figure 3.4 Dependence of Reynolds number on the parameter $Gr_{T_D} Pr(D_h/L)$.

source and the sink legs cause the packet to circulate about the loop. When the packet of fluid completes one revolution and returns to the source leg it will have gained momentum from the buoyancy forces. So, to the source leg it will appear that the packet of fluid has been forced into the leg. Yet, buoyancy forces would still exist to drive the flow, so the particle of fluid passing through the source leg will be subjected to both forced and free convection.

3.2.2 Average Heat Transfer Coefficients

Since unique parameters which control heat transfer in a natural circulation loop, as is the Rayleigh number in free convection or the Reynolds number is in forced convection, have not been identified, different dimensionless parameters were tried in correlating the average Nusselt number data. For all attempts it was found that a better correlation could be obtained by plotting against $\overline{Nu}/Pr^{0.43}$ rather than the average Nusselt number, $\overline{Nu}$, alone. This finding is consistent with the results of a previous work [8].

Figure 3.5 shows a plot of the heat transfer parameter $\overline{Nu}/Pr^{0.43}$ vs. the Reynolds number for both counter-flow and parallel-flow arrangements. For counter-flow a correlation determined on the basis of least squares fit of the data was of the form

$$\overline{Nu} = 0.026\ Re^{0.93}\ Pr^{0.43} \qquad (3.11)$$

For parallel-flow the following correlation was obtained,

$$\overline{Nu} = 0.051\ Re^{0.80}\ Pr^{0.43} \qquad (3.12)$$

The dashed lines in each of the figures represent results of Gruszczynski and Viskanta (1983) for a different tube bundle geometry. The difference between the two correlations demonstrates the dependence of the heat transfer coefficient on the geometry of the tube bundle. The reason that the average heat transfer coefficient data correlate vs. the Reynolds number is because the Grashof number (Gr_{T_D}) is nearly proportional to the Reynolds number (see Fig. 3.2).

In general, the parallel-flow arrangement resulted in higher Nusselt number than the counter-flow case for Reynolds numbers below 200. For increasing Reynolds numbers, the average Nusselt number for the counter-flow arrangement becomes progressively greater than that for the parallel-flow case. It appears that the buoyancy driving force for Reynolds numbers greater than 200 becomes progressively greater for the counter-flow case

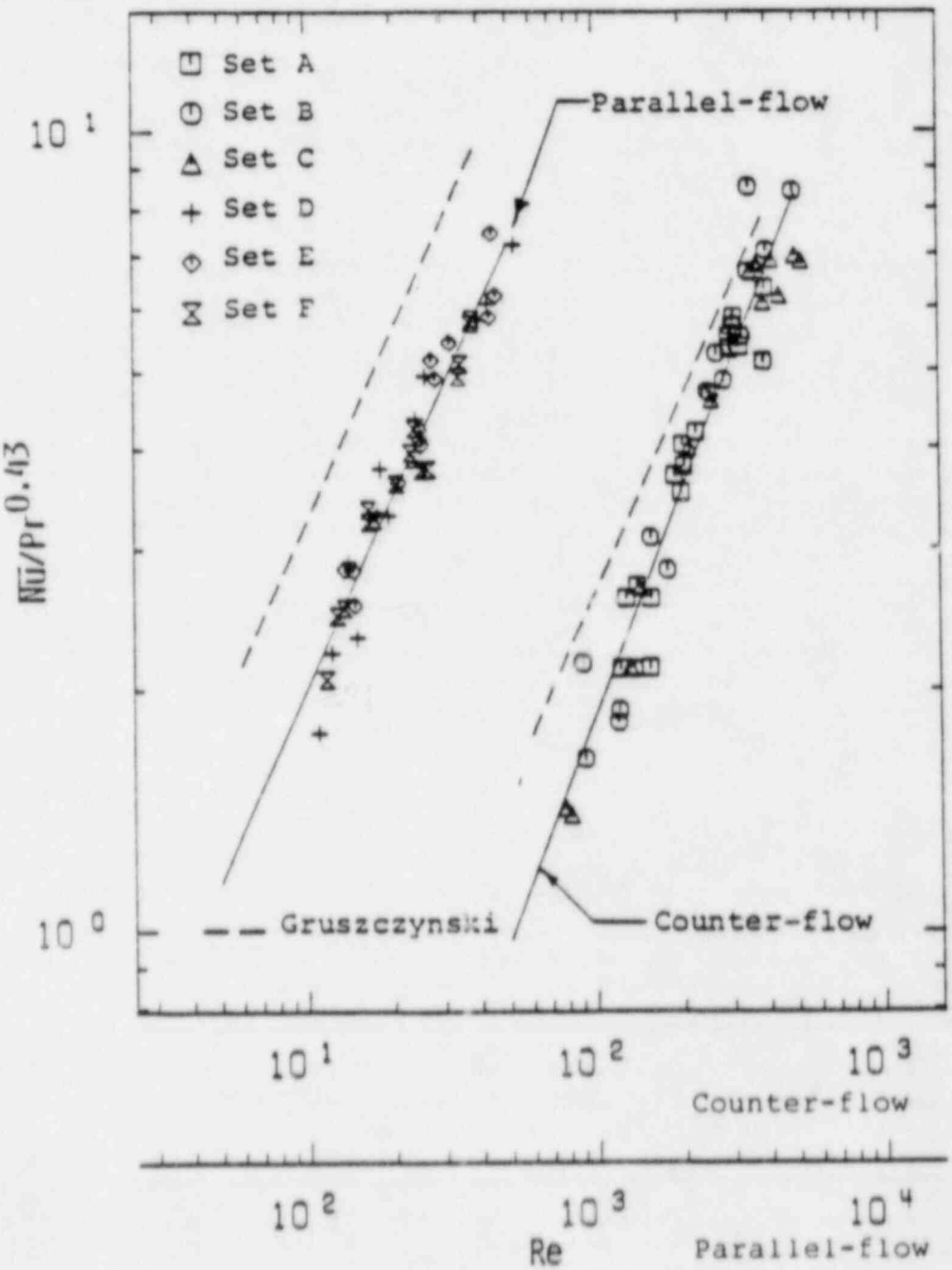

Figure 3.5 Dependence of the parameter $\overline{Nu}/Pr^{0.43}$ on the Reynolds number.

(Fig.3.2).

Another correlation for both the parallel-flow and counter-flow arrangement results from plotting $\overline{Nu}/Pr^{0.43}$ versus the modified Grashof number. Figure 3.6 shows the plots of $\overline{Nu}/Pr^{0.43}$ versus Gr_m for both flow arrangements. For counter-flow the correlation obtained from the least squares fit of the data is of the form,

$$\overline{Nu} = 0.11\ Gr_m^{0.48} Pr^{0.43}, \qquad 4 \times 10^4 < Gr_m < 10^6 \qquad (3.13)$$

For parallel-flow a similar correlation results in

$$\overline{Nu} = 0.024\ Gr_m^{0.42} Pr^{0.43}, \qquad 4 \times 10^4 < Gr_m < 10^6 \qquad (3.14)$$

In Eqs.(3.13) and (3.14) is the Grashof number based on the average heat flux in the source leg q_{so} defined as

$$Gr_m = \frac{\rho g \beta q_{so} D_h^4}{k\ \mu^2} \qquad (3.15)$$

Attempts to correlate $\overline{Nu}/Pr^{0.43}$ vs. the Grashof number

$$Gr = \frac{\rho^2 g \beta D_m^3 \Delta T_{w-L}}{\mu^2} \qquad (3.16)$$

resulted in much more scatter. Note that the exponent on the Rayleigh (Grashof) number is considerably larger than that usually expected for laminar or turbulent natural convection conditions (Eckert and Drake, 1972). The dependence of the average Nusselt number on the Rayleigh number resembles that for natural convection in porous media for which $\overline{Nu} \propto Ra^m$, where m ranges between 0.5 and 0.69 (Gabitto and Boehm, 1981). This type of Rayleigh number dependence was noted earlier for tubes in a triangular array (Gruszczynski and Viskanta, 1982) .

Since mixed convection heat transfer appears to be prevalent in the natural circulation loop, an appropriate correlation of the average Nusselt number would be in terms of both the forced and natural convection parameters, the Reynolds and Grashof numbers, respectively. Since a correlation had been obtained for the average Nusselt number vs. the Reynolds number to the 0.8 power for both flow arrangements, a plot of the Nusselt number times the Reynolds number to the 0.8 power divided by the Prandtl number to the 0.43 power versus the modified Grashof number was made, and is shown in Fig.3.7. It is apparent from this figure

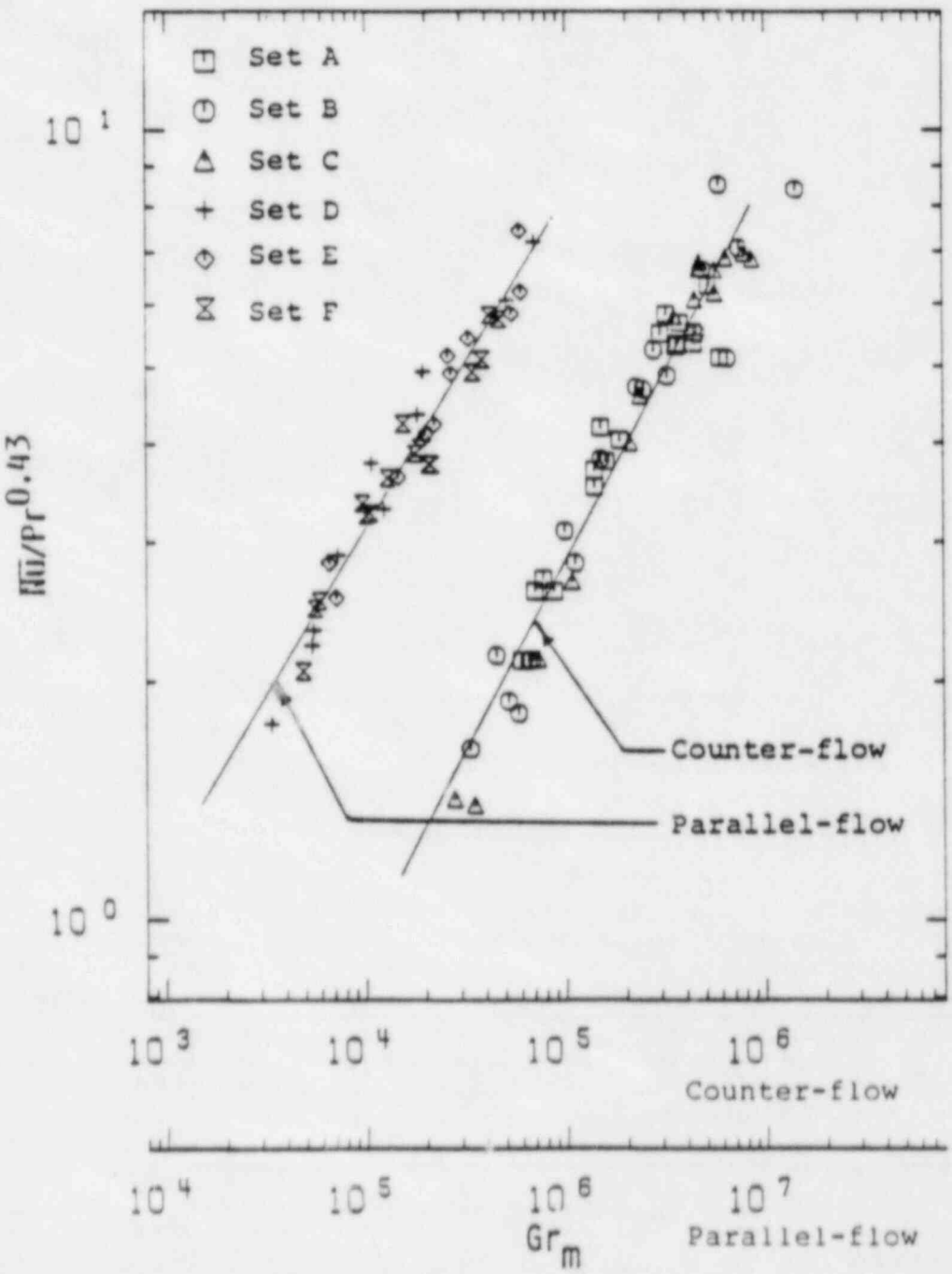

Figure 3.6 Dependence of the parameter $\overline{Nu}/Pr^{0.43}$ on the modified Grashof number.

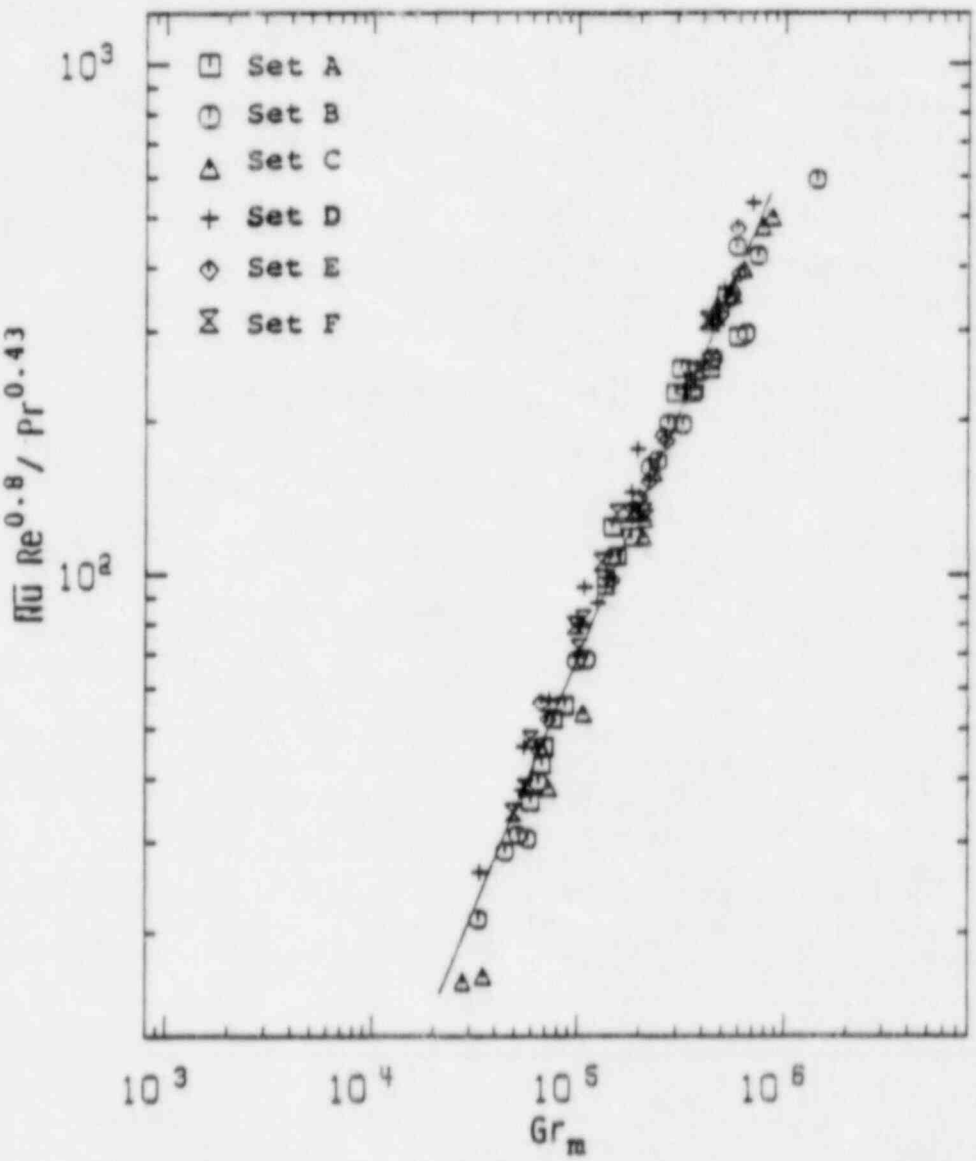

Figure 3.7 Correlation of the parameter $\overline{NuRe}^{0.8}/Pr^{0.43}$ with the modified Grashof numbers for bundle without grid spacers.

that the data from both the parallel-flow and counter-flow tests can be represented by a single curve, as given by the following correlation,

$$\overline{Nu} = 0.00091\ (Gr_m/Re)^{0.8}\ Gr_m^{0.176}\ Pr^{0.43} \qquad (3.17)$$

The success of Eq.(3.17) in correlating all of the experimental data suggests that indeed heat transfer under natural circulation conditions over a tube bundle is one of the mixed convection type. The average Nusselt number is a function of both the Reynolds and Grashof numbers. An interesting result obtained from plotting $\overline{Nu}\ Re^n/Pr^{0.43}$ vs. Gr_m for different values of m reveals little sensitivity of the correlations to the exponent n as long as n is greater than approximately 0.25.

3.3 Steady-State Test Results for a Bundle with Spacers

A set of steady-state experiments similar to those listed in Table 3.1 was performed after the egg-crate type spacers shown in Fig.2.4 were arranged on the test bundle. Only the effect of varying the heating rates was studied for each of the runs.

Flow visualization with the grid spacers arranged on the bundles did not produce any unusual results. At low heat fluxes ($Gr_m < 4.8 \times 10^5$, $Re < 320$) the effect of the grid spacer on the flow was to cause mixing in the region immediately downstream of the spacer. The streamlines (for laminar flow) would then redevelop at some distance downstream of the spacer. For greater heat fluxes, no laminar streamlines formed downstream of the spacer. The dye mixed thoroughly with the circulating fluid.

The average fluid friction results with and without grid spacers were practically the same (within experimental accuracy). These results were not surprising as the blockage ratio, ε, defined as

$$\varepsilon = \frac{A_{gs}}{A_{gs} + A_f} \qquad (3.18)$$

where A_{gs} the cross-sectional area of the spacers was only $\varepsilon = 0.2\%$ so the additional flow resistance provided by the grid spacer was minimal.

The results obtained for the average heat transfer coefficients in the tests with grid spacers differed significantly from the results obtained in the tests without the grid spacers. At similar conditions (i.e., heating rates) the average heat transfer coefficients were increased by the grid spacers. Based on the data obtained by Velcek and Weber (1970), and the

empirical correlation given by Yao et al. (1982), the ratio of the local Nusselt number downstream of a grid spacer, Nu_{gs} to the local Nusselt number which would exist if no grid spacer were present is

$$\frac{Nu_{gs}}{Nu} = 1.0 + 5.55\varepsilon^2 e^{-0.13(x/D_h)}, \quad 1\times10^4 < Re < 1.55 \times 10^5 \qquad (3.23)$$

For the blockage ratio used in these experiments and for the spacing of the grid spacers, an increase of about 5% in the average Nusselt number for the grid spacer tests above the value obtained without the grid spacers is expected using Eq.(3.15).

Figure 3.8 provides the comparison of the heat transfer coefficient enhancement due to the presence of the grid spacers, showing the relationship of the heat transfer parameter $\overline{Nu}/Pr^{0.43}$ and the Reynolds number. The correlations obtained from the tests with grid spacers on the tube bundle are

$$\overline{Nu} = 0.043\ Re^{0.86} Pr^{0.43} \qquad (3.24)$$

and

$$\overline{Nu} = 0.077\ Re^{0.75} Pr^{0.43} \qquad (3.21)$$

for counter-flow and parallel-flow arrangements, respectively. Comparison of the two cases for both counter-flow and parallel-flow arrangements reveals a flow dependence of the heat transfer enhancement. At low Reynolds numbers ($Re < 100$), an increase of nearly 20% in the average Nusselt number is obtained due to the presence of the grid spacers. In the transition regime ($Re \simeq 320$) an increase of only 10% is found. That the heat transfer enhancement due to the grid spacers diminishes as the flow becomes mixed (irregular) is not surprising. With increased mixing it would be expected that the additional mixing resulting from the presence of the grid spacers would have a negligible effect on the heat transfer as the fluid would already be well mixed under turbulent flow conditions. The conclusions reached above are reinforced by the results of Fig.3.9 showing the heat transfer parameter $\overline{Nu}/Pr^{0.43}$ vs. the modified Grashof number, although the flow dependence of the heat transfer enhancement is not evident here, possibly because the scatter of data is more pronounced. The least squares fit of the experimental data for the counter-flow and parallel-flow arrangements were, respectively,

$$\overline{Nu} = 0.016\ Gr_m^{0.488} Pr^{0.43} \qquad (3.22)$$

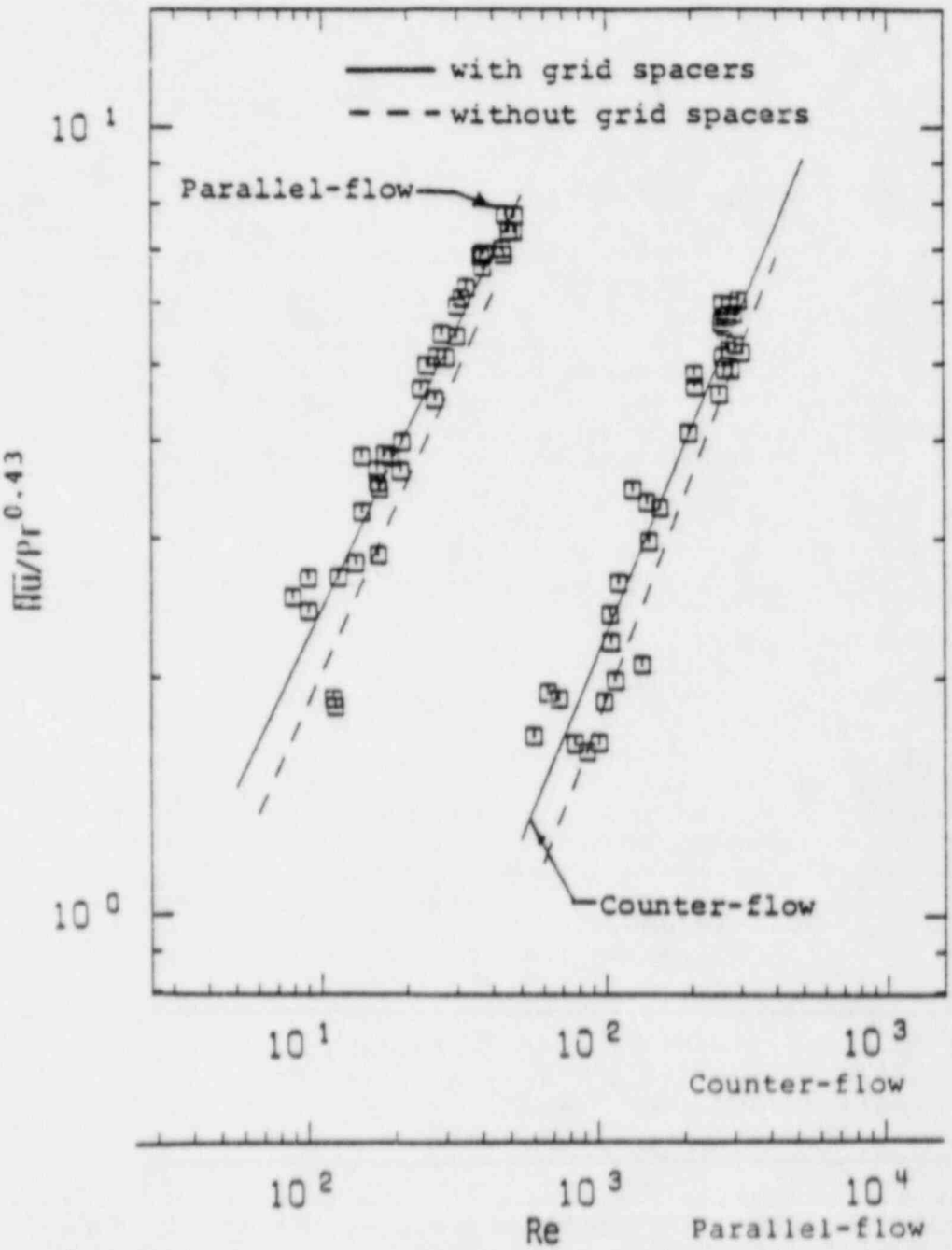

Figure 3.8 Comparison of the parameter $\overline{Nu}/Pr^{0.43}$ vs. Reynolds number for bundles without and with grid spacers.

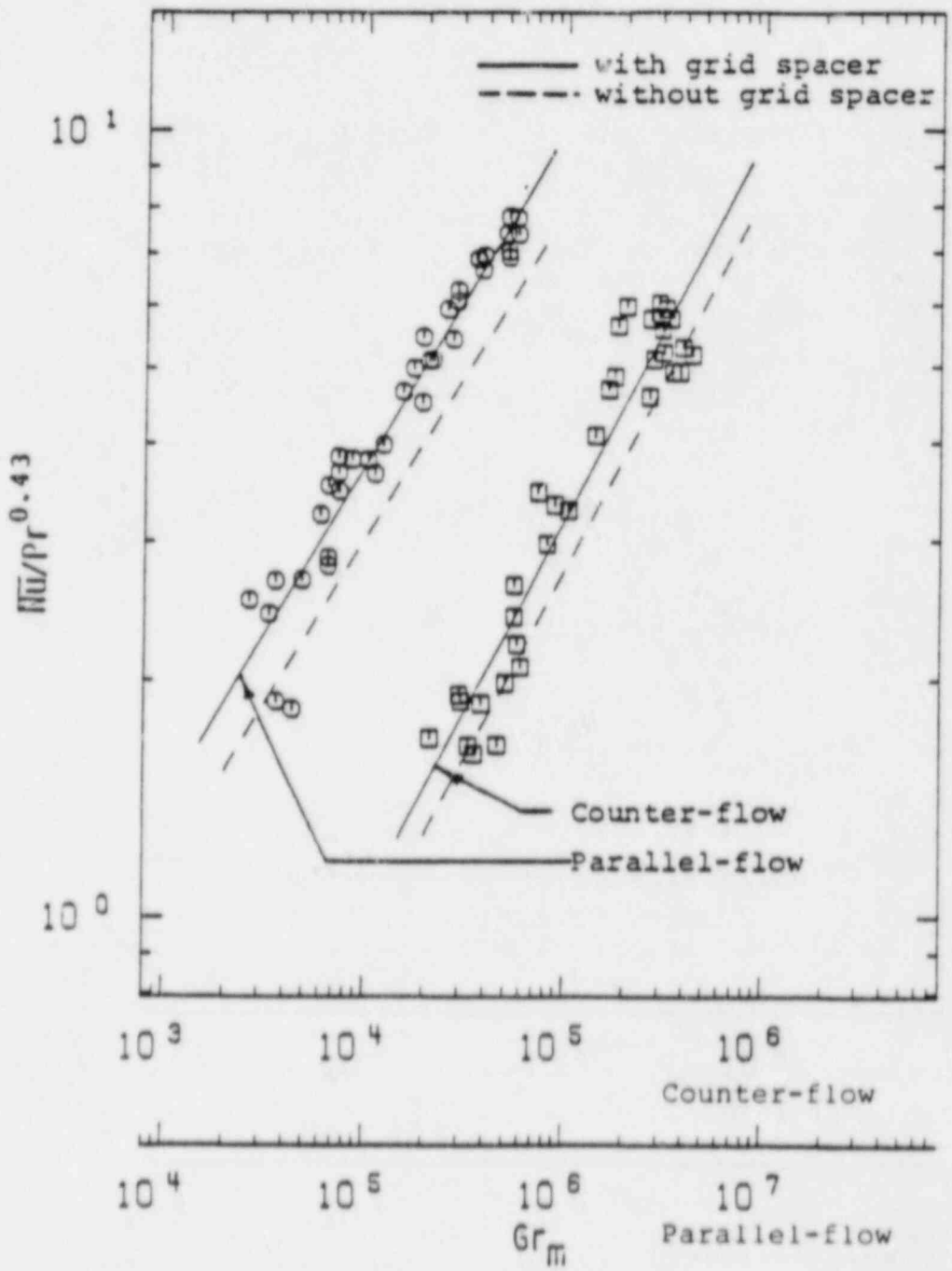

Figure 3.9 Comparison of the parameter $\overline{Nu}/Pr^{0.43}$ vs. the modified Grashof number for bundles without and with grid spacers.

and

$$\overline{Nu} = 0.072\ Gr_m^{0.428} Pr^{0.43} \qquad (3.23)$$

Again, the results show an increase in the average heat transfer coefficient at identical conditions for the tests with the grid spacers on the bundle compared to those obtained in the tests without grid spacers. Comparison of Figs.3.6 and 3.8 reveals that there is greater scatter of the experimental data for the tests with grid spacers on the bundles.

As was done for the tests without grid spacers on the tube bundles, the experimental data for both the counter-flow and parallel-flow arrangements with grid spacers were correlated by a single equation,

$$\overline{Nu} = 0.00055\ (Gr_m/Re)^{0.8} Gr_m^{0.2} Pr^{0.43} \qquad (3.24)$$

The equation is of the same form as the one for the bundle without grid spacers and differs only in the constant and the exponent of the modified Grashof number. However, the heat transfer enhancement is not evident as in the preceeding figures.

A series of natural circulation tests were conducted at a FLECHT SEASET facility which was scaled 1/307 by volume to a full size PWR (NUREG/CR-3654, 1984). The purpose of these tests was to identify hydraulic and heat transfer phenomena during single phase, two phase and reflux condensation natural circulation cooling modes. Extensive test data are reported. Data reduction, analysis, evaluations and model development are discussed. However, no heat transfer correlations for the heater rod bundle are presented. Direct comparison of flow and heat removal rates between the present natural circulation loop and the FLECHT SEASET test facility is not possible because of the diferences in the system design and test conditions.

4. DYNAMICS OF A NATURAL CIRCULATION LOOP

4.1 Analysis of Dynamic Behavior

4.1.1 Physical Model and Assumptions

A mathematical model has been developed to predict the dynamic response of a single phase natural circulation loop shown in Fig. 3.1. A one-dimensional model, where the only space coordinate, s, runs along the components of the loop is adopted to describe the spatial dependence of mass flow rate and temperature (Zvirin and Rabinoviz, 1983; Zvirin et al. 1981). The temperature is, then, the cross-sectional average in each component of the loop. The one-dimensionality assumption implies that correlations for fluid friction and heat transfer coefficients have to be obtained from the literature.

The same assumptions described in Section 3 were employed in developing the transient model equations of mass, momentum and energy for a differential volume element of fluid or structural component. Available results (Gruszczynski and Viskanta, 1983) have shown that lumping the structural components and the circulating loop fluid into a single effective energy storage term (heat capacity) yields an unsatisfactory dynamic response of the loop. Therefore, separate energy balances are made for each fluid stream and structural component of the loop. For example, in the heat source leg, energy balances are made on the working fluid, the circulating fluid, the tube bundle, the loop piping and the insulation.

4.1.2 Mathematical Model

The equation of conservation of mass for one-dimensional flow about the loop is

$$\frac{\partial \rho}{\partial t} + \frac{\partial \rho \bar{u}}{\partial s} = 0. \qquad (4.1)$$

The conservation of momentum law for the vertical legs of the loop may be expressed in terms of the mass flow rate, $G = \rho A_f \bar{u}$, and results in the following equation,

$$\frac{1}{A}\frac{\partial G}{\partial t} + \frac{G}{\rho A^2}\frac{\partial G}{\partial s} = -\frac{\partial P}{\partial s} \pm \rho_o g[1-\beta(T_f-T_o)] - \frac{f}{D_h}\frac{1}{\rho A^2}\frac{G^2}{2} \qquad (4.2)$$

The buoyancy term in Eq. (4.2) is not present in the momentum equation written for the horizontal legs.

Following the analysis of Zvirin et al. (1981), the momentum equations for each leg of the loop were integrated over their respective lengths. The resulting equations were summed yielding

$$\alpha \frac{\partial G}{\partial t} + R \frac{1}{\rho} \frac{G^2}{2} = \rho_o g \beta L_s \left[\int_0^{L_s} T_{so}(s)ds - \int_0^{L_s} T_{si}(s)dx \right] \quad (4.3a)$$

or

$$\alpha \frac{\partial G}{\partial t} = \rho_g g \beta L_s \Delta T_D - R \frac{1}{\rho} \frac{G^2}{2} \quad (4.3b)$$

where R is the effective flow resistance parameter, and is composed of the sum of the frictional and form losses (Zvirin et al., 1981), and α is the reciprocal of the flow area integrated around the loop. The parameter R for each leg is defined as

$$R = \sum_i f_i \frac{L_i}{D_{hi} A_i^2} + \sum_j \frac{K_j}{A_j^2} \quad (4.4)$$

The energy equations are written for each component of the individual legs of the loop. For the vertical leg of the loop containing tube bundle #1, the energy equations were written for the fluid flowing through the tube bundle, the tube walls of the bundle, the fluid circulating in the loop, the loop walls, and the insulation. These equations become as follows:

Working fluid

$$n(\rho c_p A)_i \frac{\partial T_i}{\partial t} + \dot{m} c_p \frac{\partial T_i}{\partial s} = \bar{h}_i P_i n(T_w - T_i) \quad (4.5)$$

Tube bundle

$$n(\rho c_p A)_w \frac{\partial T_w}{\partial t} = \bar{h}_i P_i n(T_i - T_w) = \bar{h}_o P_o n(T_w - T_f) \quad (4.6)$$

Circulating fluid

$$(\rho c_p A)_f \frac{\partial T_f}{\partial t} + G c_p \frac{\partial T_f}{\partial s} = \bar{h}_o P_o n(T_w - T_f) - \bar{h}_{ot} P_{ot} (T_f - T_t) \quad (4.7)$$

Loop tube

$$\rho c_p A_t \frac{\partial T_t}{\partial t} = \bar{h}_{ot} P_{ot} (T_f - T_t) - U_t P_t (T_t - \bar{T}_{ins}) \qquad (4.8)$$

Insulation

$$(\rho c_p A)_{ins} \frac{\partial \bar{T}_{ins}}{\partial t} = U_t P_t (T_t - \bar{T}_{ins}) - \bar{h}_a P_{ins} (T_o - T_a) \qquad (4.9)$$

A similar set of equations was written for the vertical loop leg containing tube bundle #2. The system of equations for the two connecting horizontal legs was simpler because the equations for the working fluid and bundle tubes were not needed. The equations are similar to those given by Eqs. (4.7) through (4.9). Suffice it to note that a system comprising a total of 16 equations was solved. The initial conditions of all variables are specified in the next subsection.

4.1.3 Model Parameters

The flow resistance parameter R determined from steady-state flow data for tube bundle #1 (given in Section 3) and tube bundle #2 (Gruszczynski and Viskanta, 1983) as a function of Reynolds number was used in the calculations. The parameter was calculated for each leg of the loop as a function of the instantaneous Reynolds number in Section 3. The friction factor results calculated from the flow resistance parameter data for each of the two tube bundles followed, with some scatter, the correlations reported in the literature for laminar forced flow.

The heat transfer coefficients under natural circulation conditions associated with the loop fluid $\bar{h}_o$ and $\bar{h}_{ot}$ are assumed known and independent of time and are determined from the steady-state correlations of the average Nusselt numbers for tube bundle #1 and tube bundle #2 (Gruszczynski and Viskanta, 1983). A correlation for the heat transfer coefficient on the inside of the tubes for hydrodynamically fully developed and thermally developing flow was used (Grober et al., 1961)

$$\overline{Nu}_i = 0.02\, Re^{7/12} Pr^{1/3} (D/L)^{1/3} \qquad (4.10)$$

The relative importance of the thermal resistances has been determined for a typical test at steady-state conditions [4]. The convective resistance on the circulating fluid side of the tube bundle was about a factor of two larger than the resistance on the working fluid side inside the bundle. The conductive resistance across the insulation was the largest and across the

copper tubes was the smallest.

Use of steady-state heat transfer correlations to predict convective heat transfer between the tube bundle and the fluid circulating in the loop implies that the flow can be considered as quasi-steady, that is, the flow develops much more rapidly than the thermal structure. Based on flow visualization experiments this idealization is well justified. The flow was found to develop within a matter of seconds while thermally developing over a period of approximately an hour.

4.1.4 Method of Solution

Use of an average temperature along each leg of the circulating fluid path between inlet and outlet of each component did not yield satisfactory agreement between experimental data and model predictions (Gruszczynski and Viskanta, 1983). Therefore, the model equations were not averaged spatially. Since the equations are nonlinear and could not be integrated exactly the system of equations for the six unknowns (G, T_i, T_w, T_f, T_t and T_{ins}) were solved numerically by direct integration using a finite-difference method. Forward difference approximations were used for both the spatial and temporal derivatives (Gerald, 1980).

A time step of 1.0 second and a spatial step of 0.08 m (21 nodes) was used in each leg. The thermophysical properties of the fluid in the tube bundles and the circulating fluid in the loop were based on the axially averaged "film" temperatures $\bar{T}(t)$ in each leg. For example, the average circulating fluid temperature in the vertical legs was calculated from

$$\bar{T}(t) = \frac{1}{2L} \int_0^L [T_w(s,t) + T_f(s,t)]ds. \qquad (4.11)$$

Based on the above assumptions, the loop temperatures, flow rates and heat transfer rates were calculated as functions of time for the various components. The calculations were continued (i.e., marching forward in time) until steady-state conditions were reached.

The solution of the finite difference equations required that initial conditions be specified for each of the temperatures, $T_i(s)$, $T_w(s)$, $T_f(s)$, $T_t(s)$, $T_{ins}(s)$. Arbitrary temperatures can be used for the fluid in the loop as initial conditions. For the simulation of the test conditions, the measured initial temperatures were used as the initial conditions. This was desirable because the initial phase of a transient could be simulated more accurately. For example, even in a startup transient when the fluid in the loop is initially stagnant, there are temperature variations, particularly in the vertical legs of

the loop, as a result of temperature stratification in the laboratory.

The tube bundle wall and loop wall temperatures were known from the measurements. The mean insulation temperatures were known from the exact solution for conduction across an annulus with the known inside and outside temperatures. The heat addition to the source leg and heat removal from the sink leg were determined from the measured flow rates and temperature differences across each tube bundle.

4.2 Results and Discussion

4.2.1 Test Conditions

The test conditions for six different tests discussed in the paper are listed in Table 4.1. All of the tests were performed as transient flows between two steady end conditions for both counter- and parallel-flow arrangements in the source leg. This was done because the driving temperature difference for flow circulation between the two legs is not the same for the two flow arrangements, and uniform tube bundle wall temperatures along the flow direction could not be achieved by the working fluid (water) even when forced through the bundle at high flow rates. The steady-state temperature of the inlet to the hot leg tube bundle is denoted by $T_{i,ss}$.

Table 4.1. Test conditions for dynamic tests

Test	Step Change in Heat Input	$\dot{m}_1$ (kg/s)	$\dot{m}_2$ (kg/s)	$T_{i,ss}$ (^{o}C)
CF-1	start-up	0.070	0.054	49.07
CF-2	increase	0.070	0.054	57.23
CF-3	decrease	0.120	0.055	37.05
PF-1	start-up	0.168	0.055	39.12
PF-2	increase	0.100	0.055	54.25
PF-3	decrease	0.126	0.055	44.80

The circulating fluid flow rates were not measured experimentally for reasons discussed previously, and unlike the case for steady-state conditions, the flow rate in the transient experiments could not be determined from a simple energy balance, as some of the heat transferred from the heating fluid was stored in the tube walls, the circulating fluid, the loop walls, and the insulation. However, flow visualization revealed that the circulating fluid flow rate changed quickly when first subjected

to a step change in heating and appeared to stabilize within five seconds.

Neither the flow visualization experiments nor the temperatures of the fluid measured at numerous locations around the loop provided any evidence of unstable or oscillating flow for the test conditions studied. The observations agree with the work of others (Gau and Torrence, 1981) who found for an asymmetrically heated loop (i.e., heated and cooled from the side) the flow is always stable, whereas in a non-rectangular loop (Zvirin et al., 1981) flow oscillations were observed under certain conditions. For small average heat fluxes the flow remained laminar all along the vertical length of the tube bundle. However, for average heat fluxes of 3.4 kW/m^2 radial mixing of water was observed, and for even higher fluxes mixing occurred immediately in the vicinity of the dye injection.

4.2.2 Comparison of Predictions With Test Data

Figure 4.1 shows the locations where the circulating fluid temperatures as well as the working fluid, the containment tube and the tube bundle temperatures were measured and are used to validate the model.

A comparison between the measured and predicted circulating fluid, tube bundle wall, and loop tube wall temperatures in the source leg of the loop is given in Figs. 4.2 through 4.4. These figures represent the transient tests for parallel-flow in the heat source leg of the loop for the start-up, step increase in heating rate, and step decrease in heating rate conditions, respectively. Similar results have been obtained for the counter-flow arrangement. For each transient two separate panels (for the sake of clarity) include measured and calculated temperatures vs. time. The lines denote the predictions and the symbols denote the test data. The upper panel shows the circulating fluid temperatures at the bottom (T_{f1}) and the top (T_{f2}) of the tube bundle in the source leg. The working fluid temperature at the outlet of the tube bundle (top of the bundle) is denoted by T_{i2}. The lower panel shows a comparison of the measured and predicted loop tube (T_{t3}) and the tube bundle (T_{w3}) temperatures at the mid-height of the source leg (see Fig.4.1).

Figures 4.2 and 4.3 describe the behavior of the system for the start-up transient. The loop was initially at ambient laboratory conditions (with the fluid stagnant) before flow was initiated through the tube bundles in the source and sink legs of the loop. As can be seen from the figure, after the initial transient of about six minutes, the agreement between the predicted circulating fluid temperatures T_{f1} and T_{f2} and experimental data is quite good. The relatively large discrepancy initially is in part due to the experimental difficulty in maintaining stable flow at the inlet to the tube bundle in the source leg of the

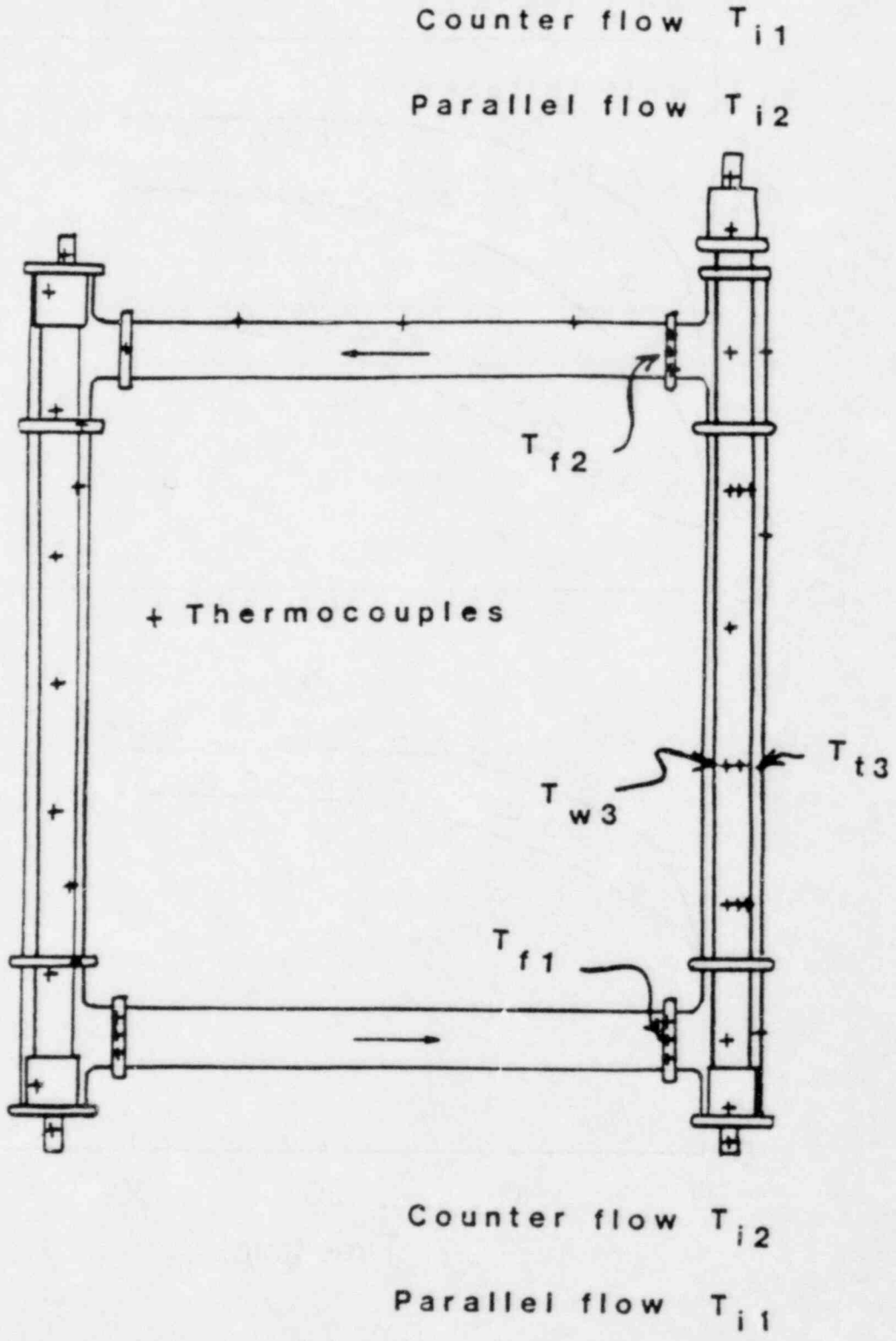

Figure 4.1 Locatins of measured temperatures in the source leg.

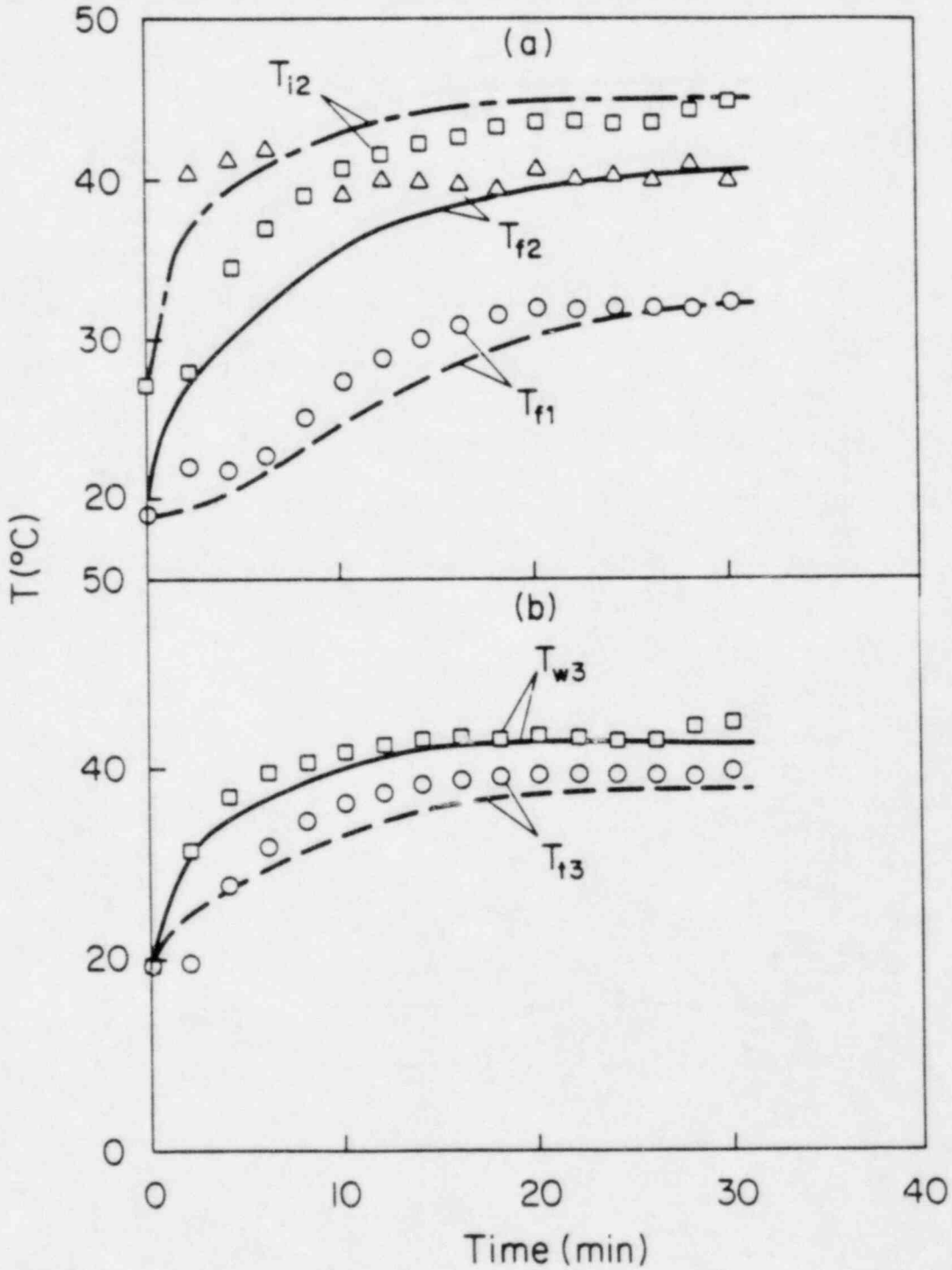

Figure 4.2 Comparison of predicted and measured temperatures for transient test P-1.

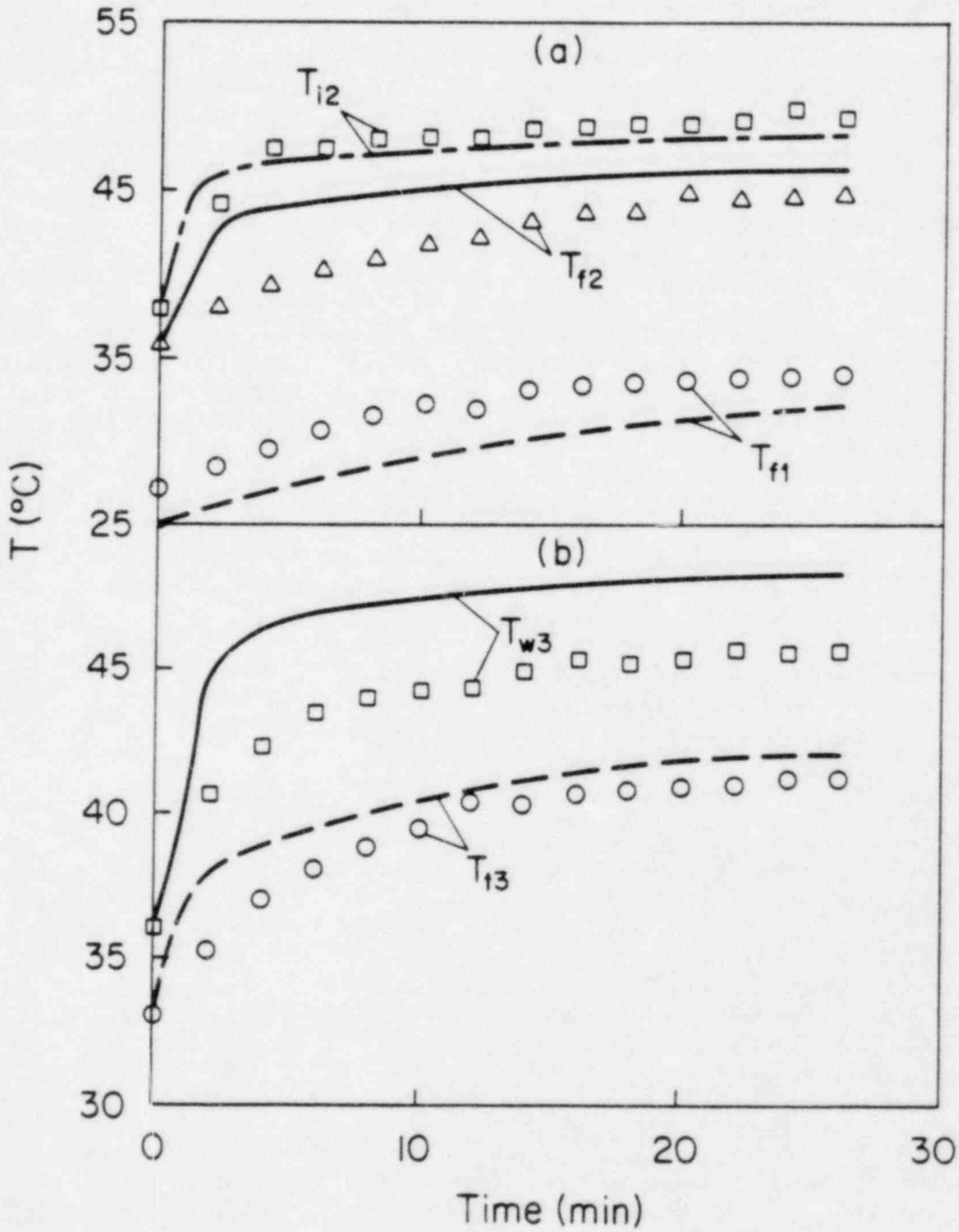

Figure 4.3 Comparison of predicted and measured temperatures for transient test P-2.

loop. Fluctuations in the inlet temperature due to poor mixing of the steam and cold water were evident in the experiment; however, these fluctuations died out as the loop heated up and steady-state conditions were approached. First, it is clear from the figure that the time constant of the transient has been correctly computed by the model. Second, very good agreement has been obtained between predicted and measured temperatures at steady state (t $\gtrsim$ 30 min).

The good agreement between measured and predicted circulating fluid temperatures at the top and bottom of the source leg supports the use of convective heat transfer coefficients between the tube bundle and the circulating fluid determined for steady state flow conditions (Gruszczynski and Viskanta, 1983) for use to predict the transient behavior of a natural circulation loop. The good correspondence between the measured and calculated tube wall temperature (T_{w3}) suggests that three-dimensional effects due to mixing of the flow in the bundle are not very significant for the test conditions. Greater tube wall temperature variations across the bundle have been observed for higher heat inputs to the system (Gruszczynski and Viskanta 1983). Finally, good agreement between the measured and predicted containment tube wall temperature indicates that the heat losses from the loop to the ambient were estimated correctly.

A comparison between the predicted and measured temperatures at the few selected locations in the source leg for the step increase and decrease in heat addition to the loop transient are given in Figs. 4.3 and 4.4, respectively. The agreement between the two sets of results is even better than for the start-up transient just discussed. The largest discrepancy is noted for the tube wall temperature for test PF-2 (Fig.4.3). The reason for this is not clear as other temperatures show good agreement. One finding which emerges from the results reported in Figs. 4.3 and 4.4 is the difference in the time constants. The observed behavior is that the time constant for test PF-2 (increase in heat addition) is greater than for test PF-3 (decrease in heat addition). This is associated with increasing and decreasing system temperatures for tests PF-2 and PF-3, respectively. The fact that the mass flow rates for tests PF-1 and PF-3 at t = 16 min are practically equal to each other is only a coincidence. The steady state is reached more rapidly in test PF-3 than PF-2 because the heat losses to the surroundings aid to accelerate the process. The reversed transition takes longer, because of heat losses from the loop to the ambient as heat addition to the system is increased.

Circulating fluid flow rates were calculated as well. Figure 4.6 illustrates the predicted flow rates for the parallel-flow arrangement for the various test runs. The results show that for the start-up and step increase in heating rate tests there was a sharp initial increase in the circulating fluid mass flow rate to a value greater than the steady-state flow rate and then a

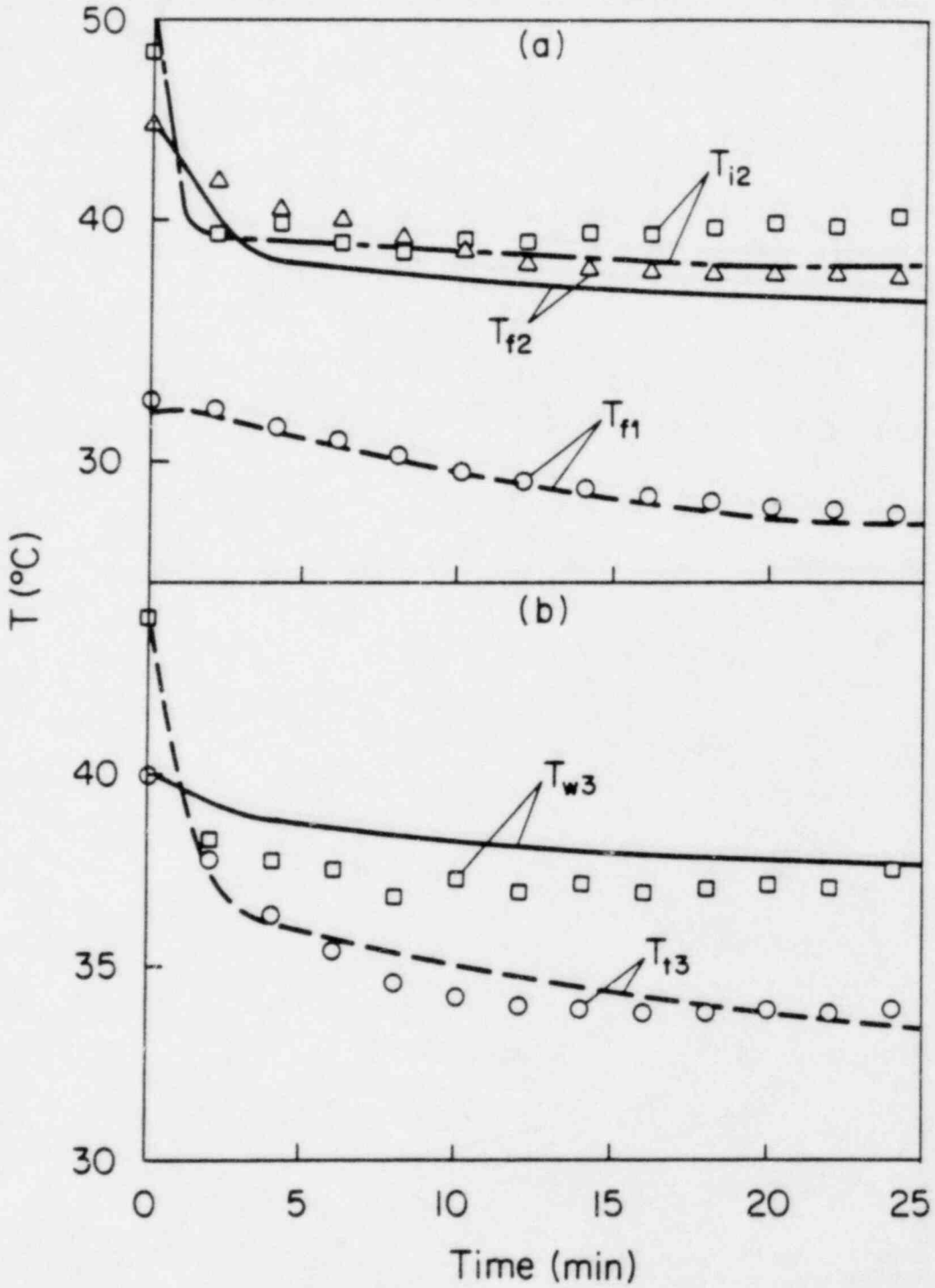

Figure 4.4 Comparison of predicted and measured temperatures for transient test P-3.

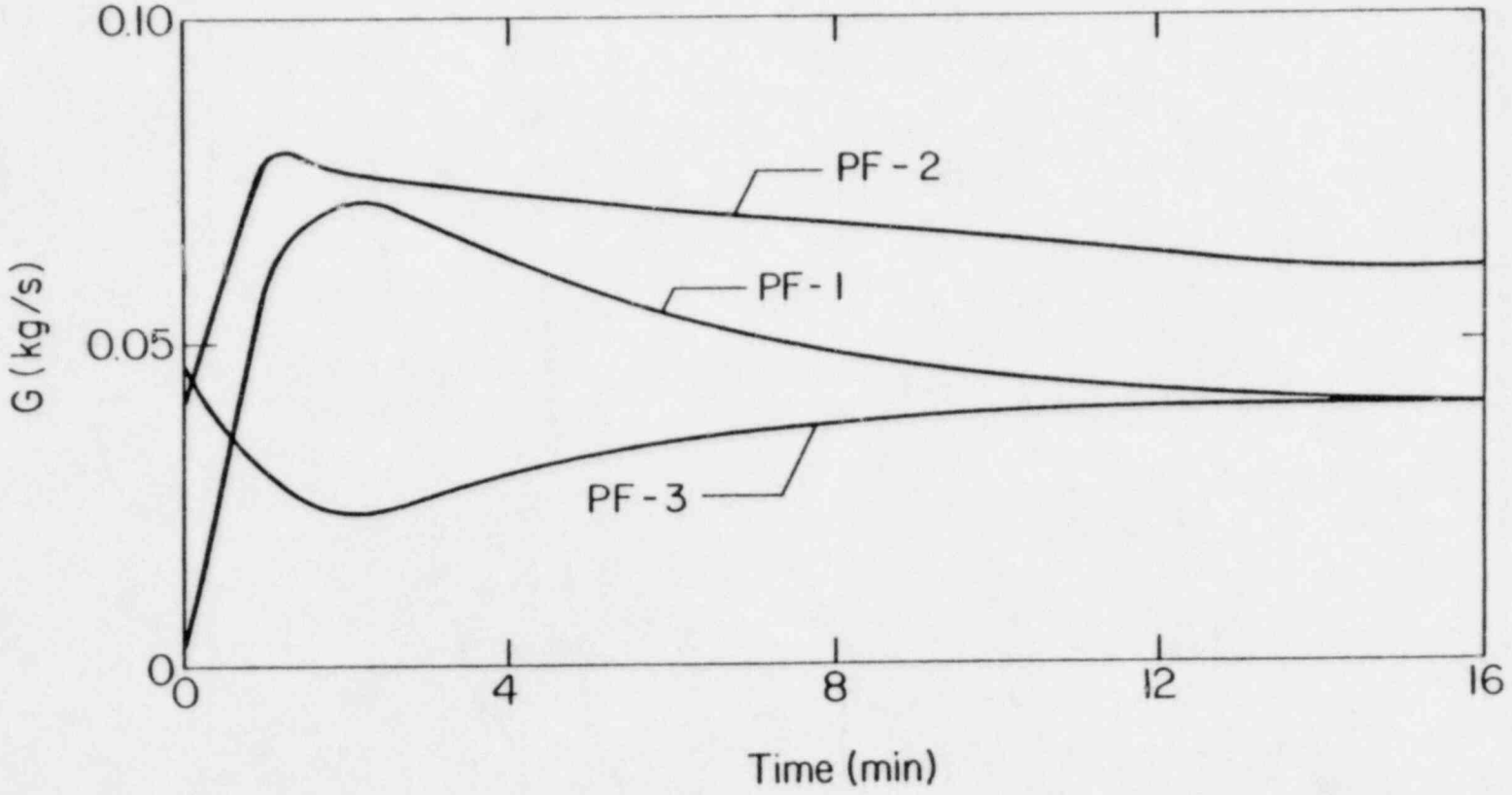

Figure 4.5 Predicted mass flow rates for parallel-flow.

gradual decrease until steady-state conditions were reached. The buoyancy driving force at the onset of flow is at a maximum initially, since the temperature difference between the heating fluid and the circulating fluid is at a maximum initially. As the temperature difference between the heating fluid (i.e., the tube walls) and the circulating fluid increases and the tube wall temperatures approach steady-state values, the temperature difference between the two legs decreases, thereby reducing the driving buoyancy force, and consequently the circulating fluid mass flow rate. Eventually, the temperature difference between the tube walls and the circulating fluid stabilizes, thereby stabilizing the flow rate.

For the tests with a step decrease in inlet heating fluid temperatures there was a sharp initial decrease in the circulating fluid flow rate followed by a gradual increase towards the steady-state value. Again, this can be attributed to a sharp initial decrease in temperature of the source leg tube walls resulting in a slight temperature difference between the tube walls and the circulating fluid. This causes the driving buoyancy force to be very small. The cooled fluid entering the source leg produced a slight increase in the temperature difference between the tube walls and the circulating fluid. This resulted in an increased buoyancy force and therefore a slightly greater mass flow rate.

Both in this paper and some recent work (Zvirin and Rabinoviz, 1983; Zvirin et al., 1981) transient response of natural circulation loops has been analyzed using a one-dimensional model. Zvirin et al. modelled the pressurized water nuclear reactor loop, which is much more complicated than the one considered in this paper; however, the model employed in this paper is more realistic in that each loop component is described in greater detail and the fluid friction and heat transfer coefficients used as model parameters have been determined for natural convection circulation rather than for forced flow conditions. The results of calculations of the two studies are similar. The main difference being that in the present system the flow is stable whereas that of Zvirin et al. (1981) indicates instabilities.

5. CONCLUSIONS

An atmospheric pressure natural circulation loop was used to measure average heat transfer coefficients to water from the tube bundle, which is prototypic of PWR fuel elements. Tests were performed with bundles without and with grid spacers. Based on the experimental results obtained, the following conclusions can be drawn:

- The heating conditions investigated resulted in stable steady-state flows.
- The natural circulation flow longitudinal to the test tube bundle was observed to be laminar when $Gr_m < 4.8 \times 10^5$ or when $Re < 340$. Above these values, radial mixing of the circulating fluid was observed. No recirculation of the flow at any of the thermal conditions studied was observed.
- The frictional resistance was determined to solely be a function of the Reynolds number and was found to accurately be predicted by forced flow relations.
- Heat transfer in the tube bundle was in a mixed-convection regime.
- Empirical correlations for the average Nusselt number were developed. A more general correlation for relating $\overline{Nu}$ to Gr/Re is suggested.
- The grid spacers used in this study ($\varepsilon = 0.24$) had no discernible effect on the fluid friction factors. However, they were found to enhance the average heat transfer coefficients over those which would be present without grid spacers, especially in the laminar flow regime.

The dynamic behavior of the laboratory test loop was observed and simulated. Based on the experimental and numerical results, the following conclusions can be drawn:

- The one-dimensional model simulated reasonably well the transient respose of a rectangular natural circulation loop with tube bundles in its vertical legs. The fluid and structural component temperatures in the source leg predicted by the model agreed well with test data. Circulating fluid flow rates were predicted also, but no conclusions regarding the accuracy of these predictions could be made because the instantaneous flow was not measured directly. Moreover, the important features of the transient steady-state behavior are depicted in the numerical results, and the time constants are predicted correctly. In general, at steady-state the predicted temperatures agreed to within 10 percent of the experimental results.

- The good correspondence between model predictions and the test data support the use of steady-state flow resistance and heat transfer coefficient correlations for transient calculations for those conditions for which quasi-steady approximation can be justified.

6. REFERENCES

Bau, H.H. and Torrance, K.E., "Transient and Steady Behavior of an Open, Symmetrically-Heated, Free Convection Loop," International Journal of Heat and Mass Transfer, 24, 597-609, 1981.

Bragina, O.N., Lel'chuck, V.L., Sorokin, A.G. and Shuyskaya, K.F., "Experimental Study of Enhancement of Heat Transfer from a Tube Bundle in Turbulent Axial Flow," Heat Transfer-Soviet Research, 13, 14-18, 1981.

Eckert, E.R.G., and Drake, R.M., Jr., Analysis of Heat and Mass Transfer, McGraw-Hill Book Co., New York, 1972.

Gabitto, J.P., and Boehm, R., "Experimental Study of Free Convective Heat Transfer in Porous Media", International Journal of Heat and Mass Transfer, 24, 1675-1679, 1981.

Gerald, C.F., Applied Numerical Analysis, 2nd Edition, Addison-Wesley Publishing Company, Inc., Reading, MA, 1980.

Grober, H., Erk, S., and Grigull, H., Fundamentals of Heat Transfer, McGraw Hill Book Co. Inc., New York, 1961.

Gruszczynski, M.J., and Viskanta, R., "Heat Transfer to Water from a Vertical Tube Bundle under Natural Circulation Conditions," Argonne National Laboratory Report, ANL-83-7, 1983.

Japikse, D., "Advances in Thermosyphon Technology," in Advances in Heat Transfer, Vol.9, Academic Press, New York, 1973, pp.1-111.

Johannsen, K., "Longitudinal Flow over Tube Bundles", in Low Reynolds Number Flow Heat Exchangers, edited by S. Kakac et al., Hemisphere Publishing Corp., Washington, DC, 1983, pp.229-273.

Johannsen, K., "Heat Exchangers Having Longitudinal Flow Over Tubes or Rods", in Low Reynolds Number Flow Heat Exchangers, edited by S. Kakac et al., Hemisphere Publishing Corp., Washington, DC, 1983, pp.275-297.

Kemeny, G.A., and Somers, E.V., "Combined Free and Forced Convection Flow in Vertical Tubes," Journal of Heat Transfer, 88, 533-544, 1962.

Marek, J. and Rehme, K., "Heat Transfer in Smooth and Roughened Rod Bundles near Spacer Grids," Fluid Flow and Heat Transfer over Rod or Tube Bundles, Edited by S. Yao and P. Pfund, ASME, New York, 1979, pp.163-170.

McKee, H.R., "Thermosiphon Reboilers: A Review", Ind. Eng. Chem., 62, 76-82, 1970.

Mertol, A. and Greif, R., "A Review of Natural Circulation Loops", in Advanced Study Institute Proceedings on Natural Convection: Fundamentals and Applications, July 1984, Izmir, Turkey.

Metais, B., Eckert, E.R.G., "Forced, Mixed, and Free Convection Regimes," Journal of Heat Transfer, 86, 295-296, 1964.

Mohanty, A.K., and Roy, D.K., "Fluid Flow Through a Circular Tube Containing Rod Cluster," Fluid Flow and Heat Transfer of Rod or Tube Bundles, Edited by S. Yao and P. Pfund, ASME, New York, 1979, pp.121-128.

Morrison, G.L., and Ranatunga, D.B.J., "Thermosyphon Circulation in Solar Collectors," Solar Energy, 24, 191-198, 1980.

Norton, B. and Probert, S.D., "Natural-Circulation Solar-Energy Stimulated Systems for Heating Water," Appl. Energy, 11, 167-196, 1982.

NUREG/CR-3654, "PWR FLECHT SEASET Systems Effects Natural Circulation and Reflex Condensation", September 1984.

Ong, K.S., "A Finite Difference Method to Evaluate the Thermal Performance of a Solar Water Heater," Solar Energy, 16, 137-147, 1974.

Rehme, K., "Low Reynolds Number Forced Convection in Tube Bundles with Uniform and Non-Uniform Power Distributions - Experimental Results and Computations", in Low Reynolds Number Flow Heat Exchangers, edited by S. Kakac et al., Hemisphere Publishing Corp., Washington, D.C., 1983, pp.299-339.

Schmid, J., "Longitudinal Laminar Flow in an Array of Circular Cylinders," International Journal of Heat and Mass Transfer, 9, 925-937, 1966.

Sparrow, E.M., and Loeffler, A.L., "Longitudinal Laminar Flow Between Cylinders Arranged in Regular Arrays," AIChE Journal, 5, 325-330, 1959.

Viskanta, R. and Mohanty, A.K., "TMI-2 Accident: Postulated Heat Transfer Mechanisms and Available Data Base", Argonne National Laboratory, Report ANL-81-26 (NUREG/CR-2121), 1981.

Vleck, J., and Weber, P., "The Experimental Investigation of a Local Heat Transfer Coefficient in the Fuel Spacer Area," Australian Atomic Energy Commission Research Establishment, LIB/TRANS 250, 1970.

Welander, P., "On the Oscillatory Instability of a Differentially Heated Fluid Loop," Journal of Fluid Mechanics, 29, 17-30, 1967.

Yang, J.M., "Analysis of Combined Convection Heat Transfer in Infinite Rod Arrays," Fluid Flow and Heat Transfer over Rod or Tube Bundles, Edited by S. Yao and P. Pfund, ASME, New York, 1979, pp.149-154.

Yao, S.C., Hochreiter, L.E. and Leech, W.J., "Heat Transfer Augmentation in Rod Bundles Near Grid Spacers," Journal of Heat Transfer, 76-81, 1982.

Zvirin, Y., "A Review of Natural Circulation Loops in Pressurized Water Reactors and Other Systems", Nuclear Eng. and Design, 67, 203-225, 1981.

Zvirin, Y., Jeuck III, P.R., Sullivan, C.W. and Duffey, R.B., "Experimental and Analytical Investigatioan of a Natural Circulation System with Parallel Loops," Journal of Heat Transfer, 103, 645-652, 1981.

Zvirin, Y. and Rabinoviz, Y., "Modeling of Natural Circulation Phenomena in Nuclear Reactor Cooling Loops", Electric Power Research Institute, NP-2951, March 1983.

APPENDIX A

Experimental Data and Heat Transfer Results

The steady-state experimental data obtained during the tests on tube bundles without and with grid spacers are tabulated in Tables A.1 and A.2. The reduced heat transfer results calculated from the experimental data are tabulated in Tables A.3 and A.4.

Table A.1 Steady-state experimental data for tests on a tube bundle without grid spacers.

Set	Q (kW)	G (kg/s)	$\dot{m}_1$ (kg/s)	$\dot{m}_2$ (kg/s)	T_a (°C)	T_b (°C)	ΔT_1 (°C)	ΔT_2 (°C)	$\bar{T}_w$ (°C)	$\bar{T}_{so}$ (°C)	$\bar{T}_{si}$ (°C)
A-1	2.31	.040	.154	.047	50.5	46.9	3.58	13.4	46.3	41.9	40.1
A-2	2.31	.040	.154	.047	49.5	46.0	3.59	13.4	45.4	40.8	39.4
A-3	2.55	.041	.144	.047	52.8	48.5	4.22	14.1	48.2	43.2	41.2
A-4	2.55	.041	.144	.047	52.9	48.7	4.22	14.4	48.4	43.2	41.2
A-5	3.10	.046	.137	.047	56.8	51.4	5.41	17.7	51.8	45.4	43.9
A-6	2.32	.040	.154	.047	50.2	46.6	3.61	13.5	46.0	41.4	39.5
A-7	2.13	.042	.135	.046	47.2	43.4	3.77	11.6	44.1	40.3	38.2
A-8	2.13	.042	.140	.046	45.6	42.0	3.64	10.9	42.6	38.6	36.7
A-9	3.06	.050	.130	.046	51.8	46.2	5.60	15.1	48.0	43.1	41.2
A-10	.815	.023	.149	.046	32.3	31.0	1.30	3.95	30.4	27.2	26.0
A-11	1.35	.033	.146	.046	37.8	35.6	2.20	6.49	35.2	31.4	29.9
A-12	1.49	.031	.142	.046	42.6	40.0	2.51	9.25	39.7	35.9	33.6
A-13	1.25	.030	.144	.044	38.9	36.8	2.08	7.55	36.6	33.3	30.8
A-14	1.38	.032	.143	.043	39.9	37.6	2.31	9.01	37.6	34.0	30.8
A-15	.849	.025	.145	.044	33.7	32.3	1.39	4.89	31.9	28.8	26.6
A-16	1.52	.039	.140	.045	36.2	33.6	2.59	5.89	33.9	30.4	26.6
A-17	.879	.030	.149	.045	30.4	29.0	1.40	3.23	28.2	24.5	23.4
A-18	.715	.023	.144	.047	32.0	30.8	1.18	3.71	30.0	26.7	25.1
A-19	.966	.028	.126	.047	33.7	31.9	1.83	4.58	32.0	28.5	26.7
B-1	3.10	.049	.154	.090	49.7	44.9	4.81	7.13	44.8	39.9	38.3
B-2	3.68	.053	.131	.091	52.6	45.9	6.74	8.28	48.6	43.2	40.3
B-3	3.44	.051	.135	.091	52.4	46.3	6.08	7.94	47.1	41.7	39.9
B-4	3.21	.052	.149	.090	49.0	43.9	5.15	7.45	44.2	39.3	37.8
B-5	2.60	.045	.140	.090	45.8	41.4	4.44	6.08	42.0	37.5	35.2
B-6	1.82	.034	.154	.090	42.2	39.4	2.83	5.03	38.2	33.7	31.1
B-7	.396	.012	.149	.091	26.8	26.2	.634	1.10	25.4	22.7	21.4
B-8	.487	.016	.149	.090	28.2	27.4	.779	1.39	26.4	23.1	21.2
B-9	2.03	.041	.145	.090	41.9	38.5	3.36	5.15	38.4	34.1	31.8
B-10	3.18	.056	.141	.090	47.8	42.4	5.38	6.55	43.4	38.0	36.6
B-11	3.66	.060	.142	.117	50.3	44.2	6.15	8.16	46.1	39.9	38.1
B-12	4.22	.062	.126	.090	56.4	48.3	8.01	10.1	51.1	44.8	42.8
B-13	4.43	.063	.126	.090	58.1	49.7	8.40	11.3	52.7	45.9	43.5
B-14	1.15	.025	.154	.079	37.3	35.5	1.79	3.45	33.0	28.7	26.4
B-15	.878	.025	.138	.088	31.9	30.4	1.52	2.36	30.1	26.0	24.5
C-1	1.67	.039	.154	.087	38.5	41.7	44.3	2.60	4.75	34.2	31.0
C-2	3.23	.055	.130	.085	49.8	53.7	59.6	5.91	9.36	45.1	40.5
C-3	6.91	.100	.126	.065	61.8	67.0	80.1	13.0	20.1	54.6	51.3
C-4	1.79	.038	.140	.092	40.0	43.7	46.7	3.06	5.20	35.9	32.0
C-5	.906	.028	.149	.096	28.8	30.9	32.4	1.45	1.84	25.6	23.3
C-6	1.47	.036	.142	.096	34.7	37.6	40.1	2.48	3.22	30.6	27.5
C-7	1.82	.040	.135	.096	37.3	40.7	43.9	3.22	4.41	33.1	29.3
C-8	2.10	.042	.134	.096	40.8	44.5	48.2	3.74	5.17	36.4	32.4
C-9	2.06	.041	.137	.098	40.4	43.7	47.3	3.58	5.05	36.2	32.2
C-10	2.41	.046	.145	.101	42.4	46.0	50.0	3.99	5.43	37.8	33.9
C-11	3.20	.056	.131	.088	48.3	52.8	58.7	5.85	8.19	42.5	38.8
C-12	3.29	.056	.140	.090	50.3	55.0	60.6	5.62	8.70	44.5	40.3
C-13	.814	.026	.132	.087	29.1	31.1	32.6	1.47	2.13	26.1	23.6
C-14	.874	.029	.154	.108	27.6	29.5	30.9	1.35	1.34	24.8	22.8

Table A.1 (Continued)

D-1	1.03	.029	.093	.045	34.9	37.1	39.8	2.65	5.97	31.9	29.3
D-2	1.22	.034	.093	.045	36.0	38.5	41.6	3.14	6.29	32.7	30.1
D-3	1.44	.039	.098	.044	36.5	39.2	42.8	3.51	7.48	33.0	30.5
D-4	1.54	.037	.093	.044	38.5	41.9	45.9	3.95	8.49	34.6	31.9
D-5	1.69	.040	.093	.044	40.4	44.1	49.4	4.33	10.1	35.6	32.6
D-6	1.65	.038	.098	.047	41.2	44.7	48.7	4.04	9.14	36.5	33.6
D-7	2.35	.045	.098	.047	47.3	51.4	57.1	5.73	12.8	42.3	38.9
D-8	2.66	.048	.098	.047	48.9	53.1	59.6	6.49	15.2	43.9	40.2
D-9	2.62	.051	.098	.051	46.5	50.8	57.2	6.41	12.8	41.8	38.7
D-10	1.53	.035	.088	.044	39.8	43.0	47.2	4.15	8.65	35.9	32.8
D-11	2.30	.047	.093	.044	45.1	49.2	55.1	5.89	12.7	40.3	37.1
D-12	1.02	.028	.088	.049	34.0	36.7	39.4	2.77	5.17	30.8	28.2
D-13	1.01	.029	.090	.050	33.2	35.7	38.4	2.70	4.60	30.3	27.8
D-14	.757	.026	.090	.046	28.2	30.2	32.2	2.00	3.12	25.6	23.6
D-15	.716	.025	.092	.045	28.3	30.2	32.0	1.86	2.97	25.4	23.2
D-16	.640	.023	.096	.045	27.7	29.2	30.8	1.60	2.76	25.0	23.0
E-1	3.30	.046	.091	.046	58.6	50.0	8.68	17.9	52.9	45.9	45.5
E-2	4.89	.047	.088	.046	75.3	62.2	13.1	30.2	65.0	58.1	56.8
E-3	3.17	.043	.098	.046	57.6	49.8	7.73	18.8	51.3	44.2	44.8
E-4	2.21	.039	.098	.046	47.9	42.5	5.40	12.9	44.0	39.5	37.7
E-5	1.88	.038	.098	.046	44.1	39.5	4.60	10.6	41.0	37.0	35.4
E-6	1.00	.026	.093	.046	35.7	33.1	2.57	6.33	33.8	30.7	28.9
E-7	1.16	.031	.098	.046	35.7	32.9	2.84	6.06	33.6	29.6	28.6
E-8	.785	.025	.093	.046	31.4	29.4	2.01	4.00	29.9	26.4	25.5
E-9	.461	.019	.094	.046	27.9	26.7	1.17	2.51	26.3	23.3	22.9
E-10	.339	.017	.093	.046	31.2	29.8	1.38	3.84	29.6	26.9	25.9
E-11	2.05	.039	.091	.046	46.2	40.8	5.37	11.6	42.0	37.6	37.8
E-12	1.38	.034	.093	.046	38.9	35.3	3.54	7.71	36.3	32.5	32.1
E-13	1.81	.037	.091	.046	43.1	38.3	4.75	10.8	40.0	35.9	35.5
E-14	2.63	.042	.093	.046	52.6	45.9	6.75	15.3	48.3	43.3	41.0
E-15	2.91	.045	.093	.044	52.9	45.5	7.47	17.7	47.7	42.6	43.0
E-16	3.60	.046	.088	.046	60.4	50.7	9.72	20.8	53.7	47.6	48.0
E-17	.659	.023	.090	.045	30.2	28.5	1.74	3.35	28.6	25.1	24.5
E-18	.688	.022	.085	.045	32.1	30.2	1.93	4.24	30.3	26.7	25.0
F-1	.477	.023	.158	.044	25.4	26.8	27.5	.719	2.12	23.0	21.4
F-2	.664	.023	.156	.044	29.2	30.9	31.9	1.01	3.81	26.5	24.1
F-3	.815	.025	.158	.044	31.5	33.4	34.6	1.22	4.92	28.8	26.3
F-4	.708	.029	.158	.044	28.2	29.5	30.5	1.06	3.39	25.5	23.3
F-5	1.09	.031	.154	.044	33.8	36.2	37.9	1.70	6.78	31.0	28.2
F-6	1.56	.038	.159	.044	38.5	41.9	44.2	2.34	8.82	34.9	31.9
F-7	1.61	.040	.163	.043	39.1	42.3	44.6	2.36	6.51	35.8	33.0
F-8	1.07	.032	.135	.047	32.7	35.0	36.9	1.89	4.29	29.6	27.6
F-9	1.23	.033	.134	.050	34.8	37.4	39.6	2.19	5.77	31.2	28.7
F-10	2.75	.053	.163	.050	47.0	50.8	54.8	4.02	13.2	42.0	38.8
F-11	2.90	.054	.157	.051	49.0	52.9	57.3	4.42	14.5	44.0	40.5
F-12	3.50	.062	.140	.052	52.5	56.8	62.8	5.97	16.5	47.2	43.7

Table A.2 Steady-state experimental data for tests on a tube bundle with grid spacers.

Set	Q (kW)	G (kg/s)	$\dot{m}_1$ (kg/s)	$\dot{m}_2$ (kg/s)	T_a (°C)	T_b (°C)	ΔT_1 (°C)	ΔT_2 (°C)	$\bar{T}_w$ (°C)	$\bar{T}_{so}$ (°C)	$\bar{T}_{si}$ (°C)
GC-1	.586	.018	.275	.038	30.2	29.7	.509	4.26	28.3	25.3	23.4
GC-2	.673	.019	.266	.041	31.6	31.0	.605	4.88	29.5	26.7	24.5
GC-3	.950	.026	.261	.039	33.1	32.2	.869	5.58	30.7	27.6	25.9
GC-4	.963	.025	.252	.039	35.0	34.1	.914	6.59	32.3	29.4	27.3
GC-5	1.08	.027	.252	.039	36.1	35.1	1.03	7.08	33.2	30.0	28.0
GC-6	1.40	.033	.243	.038	37.8	36.4	1.38	7.78	34.6	31.2	29.7
GC-7	1.53	.034	.233	.040	39.6	38.1	1.57	8.87	36.0	32.7	30.9
GC-8	1.55	.033	.233	.038	41.1	39.5	1.59	9.96	37.3	34.0	32.2
GC-9	2.05	.039	.224	.037	45.3	43.1	2.19	12.0	40.8	37.1	35.5
GC-10	2.29	.042	.219	.037	46.1	43.6	2.50	12.9	41.2	37.1	35.8
GC-11	1.88	.036	.210	.036	46.7	44.5	2.14	10.5	42.9	38.7	35.3
GC-12	1.96	.036	.196	.034	48.9	46.5	2.39	12.6	45.3	41.6	36.4
GC-13	2.02	.034	.182	.031	52.7	50.1	2.66	15.6	48.0	43.5	38.9
GC-14	2.21	.036	.177	.030	53.9	50.9	2.98	16.5	48.9	44.4	39.5
GC-15	2.31	.037	.172	.030	55.8	52.6	3.20	17.6	50.8	45.9	40.9
GC-16	2.12	.035	.177	.048	54.2	51.4	2.86	17.1	49.2	44.5	40.2
GC-17	2.07	.036	.196	.048	51.1	48.5	2.50	15.1	46.6	42.6	38.3
GC-18	2.05	.037	.205	.047	48.9	46.5	2.39	14.0	45.8	40.7	37.5
GC-19	2.09	.037	.205	.046	49.0	46.5	2.44	14.4	44.9	41.1	37.5
GC-20	1.92	.036	.215	.044	47.4	45.3	2.14	13.6	43.6	39.6	37.1
GC-21	2.23	.044	.229	.042	45.1	42.7	2.34	12.2	41.3	37.4	36.3
GC-22	1.85	.044	.289	.046	36.9	35.4	1.53	6.88	34.0	30.7	29.8
GC-23	1.89	.042	.271	.042	39.1	37.4	1.67	8.81	35.9	32.7	30.3
GC-24	.834	.023	.275	.039	33.1	32.3	.724	5.85	30.9	28.5	26.6
GC-25	.667	.019	.275	.036	33.0	32.4	.579	5.70	30.7	27.7	26.2
GC-26	.692	.021	.285	.042	30.7	30.1	.581	4.37	28.7	26.1	25.1
GC-27	.382	.012	.289	.042	29.7	29.4	.315	3.97	28.0	25.8	23.9
GC-28	.657	.021	.294	.041	29.5	29.0	.534	4.00	27.8	24.8	22.9
GC-29	.488	.017	.252	.038	27.9	27.5	.462	3.40	27.0	23.2	22.9
GC-30	.402	.013	.247	.035	28.8	28.4	.389	3.95	27.2	24.9	22.7
GC-31	.449	.015	.294	.027	28.4	28.0	.365	3.70	26.9	24.2	23.0
GC-32	.305	.011	.299	.034	26.5	26.3	.244	2.93	25.1	23.2	21.5
GC-33	.542	.020	.313	.039	27.0	26.6	.414	3.00	25.6	23.0	21.8
GC-34	.770	.026	.303	.037	29.9	29.3	.607	4.24	28.2	25.0	23.5

Table A.2 (Continued)

D-1	1034.	6.58	173.	56.1	5.09	10.5	7.78	2.42	.982
D-2	1226.	7.23	207.	43.5	4.98	13.0	8.59	2.75	1.04
D-3	1441.	8.44	239.	29.9	4.93	15.6	7.92	2.85	.942
D-4	1541.	7.58	239.	33.6	4.72	17.9	8.87	3.63	.976
D-5	1691.	7.24	265.	32.3	4.55	20.9	10.5	4.49	1.08
D-6	1658.	7.15	253.	32.2	4.45	21.3	9.55	4.58	.948
D-7	2350.	9.15	344.	28.4	3.87	38.3	15.5	6.41	1.20
D-8	2664.	10.1	375.	29.1	3.73	46.3	18.9	6.96	1.36
D-9	2627.	10.4	379.	22.1	3.93	41.7	14.7	6.02	1.16
D-10	1539.	7.61	232.	43.0	4.57	18.9	10.7	3.73	1.11
D-11	2301.	9.01	341.	23.4	4.07	34.5	12.5	5.79	1.06
D-12	1028.	6.61	166.	56.7	5.21	10.1	7.20	2.33	.947
D-13	1019.	6.90	165.	51.6	5.31	9.71	6.52	2.16	.987
D-14	757.	5.46	135.	54.8	5.98	5.91	4.65	1.63	.782
D-15	716.	5.34	128.	62.3	5.98	5.60	4.73	1.62	.794
D-16	640.	4.47	117.	65.9	6.07	4.89	4.19	1.60	.722

E-1	1677.	7.54	251.	25.9	4.74	19.4	7.56	3.86	.839
E-2	3235.	13.2	442.	28.9	3.64	58.7	26.1	6.79	1.80
E-3	6916.	17.8	982.	8.39	2.92	182.	37.2	15.6	1.73
E-4	1795.	8.42	249.	45.4	4.56	22.1	13.0	4.01	1.34
E-5	906.	5.70	148.	48.9	5.94	7.16	4.94	1.88	.819
E-6	1477.	7.04	210.	38.6	5.19	14.6	7.89	3.09	1.02
E-7	1825.	8.37	249.	31.8	4.88	20.1	9.09	3.63	1.06
E-8	2104.	9.01	281.	34.5	4.48	26.7	12.5	4.41	1.26
E-9	2063.	9.53	273.	33.3	4.52	25.8	11.4	4.04	1.16
E-10	2414.	9.88	316.	28.2	4.32	32.6	13.0	4.92	1.22
E-11	3202.	10.3	433.	18.2	3.81	53.6	15.8	7.73	1.18
E-12	3297.	10.5	455.	17.1	3.65	59.6	16.4	8.40	1.13
E-13	814.	5.24	136.	49.2	5.88	6.55	4.19	1.85	.682
E-14	874.	6.35	146.	40.0	6.08	6.65	3.96	1.60	.684

F-1	477.	3.92	109.	56.3	6.39	3.34	3.11	1.29	.589
F-2	664.	4.75	122.	74.7	5.85	5.39	5.15	1.68	.831
F-3	815.	6.02	140.	66.3	5.52	7.29	6.03	1.84	.877
F-4	708.	5.02	130.	55.9	5.99	5.52	5.82	1.60	.979
F-5	1095.	7.69	182.	55.5	5.22	10.7	8.48	2.17	1.11
F-5	1560.	8.49	240.	45.9	4.69	18.3	12.2	3.27	1.34
F-6	1613.	9.53	259.	43.0	4.61	19.5	13.3	3.16	1.41
F-7	1073.	6.85	178.	39.3	5.38	9.99	5.74	2.18	.801
F-8	1234.	6.69	194.	33.6	5.15	12.4	5.86	2.80	.754
F-9	2750.	10.4	398.	19.0	3.89	44.4	13.9	6.38	1.08
F-10	2904.	10.7	426.	16.5	3.72	50.7	13.8	7.00	.998
F-11	3502.	12.2	526.	11.9	3.45	69.6	15.2	8.49	.956

Table A.3. Steady-state heat transfer results for tests on a tube bundle without grid spacers.

Set	Q (W)	$\overline{Nu}$	Re	RxA_f^2	Pr	Gr_m (x10^4)	Gr_{T_D} (x10^3)	Gr (x10^4)	Tdrive °C
A-1	2310.	10.2	301.	33.3	3.93	36.7	13.9	5.53	1.10
A-2	2314.	9.67	295.	30.3	4.03	35.3	12.2	5.56	1.01
A-3	2558.	9.81	321.	35.0	3.79	43.3	16.6	6.67	1.23
A-4	2558.	9.49	320.	32.2	3.78	43.4	15.2	6.92	1.13
A-5	3105.	8.86	385.	23.0	3.55	58.8	15.7	9.79	1.04
A-6	2326.	9.68	296.	32.1	3.97	36.3	12.9	5.75	1.04
A-7	2136.	10.7	305.	29.7	4.11	31.4	12.7	4.38	1.10
A-8	2132.	10.3	293.	23.8	4.27	29.4	9.46	4.26	.872
A-9	3060.	11.2	391.	20.4	3.80	51.5	14.4	6.67	1.08
A-10	615.	5.50	126.	51.2	5.70	69.1	3.79	1.98	.584
A-11	1051.	7.10	198.	30.8	5.11	13.7	5.61	2.99	.712
A-12	1494.	7.78	202.	44.0	4.58	18.3	8.28	3.65	.864
A-13	1258.	7.33	188.	51.2	4.90	13.7	8.39	2.83	.991
A-14	1387.	7.47	203.	47.1	4.81	15.6	9.01	3.16	1.02
A-15	849.	5.61	138.	68.8	5.50	7.64	6.05	2.12	.875
A-16	1520.	8.56	225.	32.4	5.25	14.7	7.55	2.67	1.00
A-17	879.	4.63	153.	40.0	6.06	6.72	4.34	2.18	.746
A-18	715.	4.52	120.	71.3	5.77	5.93	4.80	2.09	.756
A-19	966.	5.42	155.	51.3	5.50	8.67	5.70	2.40	.826
B-1	3304.	8.78	389.	21.9	3.49	64.4	15.3	10.8	.981
B-2	4894.	13.0	421.	30.7	2.76	142.	34.3	16.3	1.45
B-3	3172.	14.7	347.	42.8	3.61	58.2	23.8	10.4	1.62
B-4	2214.	8.98	282.	35.8	4.16	31.9	13.2	5.22	1.16
B-5	1887.	8.89	254.	29.6	4.45	24.3	8.84	4.03	.875
B-6	1005.	6.32	155.	42.1	5.24	9.80	4.66	2.31	.619
B-7	1164.	5.80	177.	31.2	5.32	11.0	4.52	2.93	.619
B-8	785.	4.52	135.	32.6	5.80	6.46	2.75	2.21	.438
B-9	461.	3.63	91.1	69.4	6.30	3.30	2.65	1.66	.489
B-10	539.	4.59	89.6	83.3	5.79	4.45	3.08	1.73	.488
B-11	2054.	9.89	266.	29.4	4.36	27.3	9.63	4.53	.921
B-12	1383.	7.63	205.	30.9	4.97	14.7	6.00	3.11	.725
B-13	1810.	9.05	246.	29.0	4.56	22.3	8.13	3.93	.843
B-14	2653.	9.76	328.	24.8	3.78	44.7	12.3	6.69	.912
B-15	2916.	11.8	343.	27.1	3.84	48.3	14.7	6.68	1.11
C-1	3608.	11.9	397.	28.8	3.39	73.8	20.9	10.1	1.27
C-2	639.	4.08	119.	63.0	5.99	5.13	4.14	2.06	.697
C-3	688.	3.87	118.	66.2	5.75	5.74	4.28	2.30	.670
C-4	3102.	12.2	351.	26.3	4.10	45.8	14.9	5.69	1.27
C-5	3686.	12.1	413.	19.8	3.77	62.8	15.6	7.44	1.15
C-6	3446.	11.9	382.	22.7	3.91	55.4	15.3	6.94	1.20
C-7	3219.	12.5	368.	19.8	4.16	46.4	12.3	5.64	1.08
C-8	2604.	10.9	305.	24.2	4.36	34.6	10.3	4.77	.994
C-9	1822.	7.86	212.	45.1	4.78	20.7	9.41	4.02	1.06
C-10	396.	3.17	78.0	122.	6.42	2.75	3.42	1.45	.651
C-11	487.	3.08	81.4	126.	6.30	3.48	3.86	1.82	.711
C-12	2031.	8.99	255.	26.2	4.75	23.3	7.89	3.96	.881
C-13	3181.	11.3	388.	17.6	4.27	43.9	12.2	5.83	1.12
C-14	3665.	11.3	441.	14.0	4.03	55.7	12.6	7.39	1.05
C-15	4223.	12.0	499.	18.4	3.60	77.9	21.2	9.30	1.44
C-16	4431.	11.7	525.	15.9	3.50	86.1	20.2	10.5	1.30
C-17	1158.	5.55	142.	84.3	5.43	10.6	7.83	3.04	1.10
C-18	878.	4.56	130.	73.9	5.81	7.20	5.79	2.54	.924

Table A.3 (Continued)

GP-1	.963	.025	.299	.051	31.2	32.9	33.7	.771	4.88	28.8	25.2
GP-2	1.22	.034	.289	.048	32.1	34.0	35.0	1.01	5.53	29.1	26.9
GP-3	1.25	.033	.266	.041	33.9	36.0	37.1	1.12	7.51	30.8	28.2
GP-4	1.48	.038	.261	.043	35.1	37.3	38.7	1.36	7.80	32.0	29.5
GP-5	1.58	.038	.238	.042	36.5	39.0	40.6	1.59	8.75	33.3	30.6
GP-6	1.66	.039	.224	.042	38.0	40.6	42.4	1.78	9.75	34.4	31.5
GP-7	2.01	.045	.210	.040	40.1	43.1	45.4	2.29	11.7	36.6	33.9
GP-8	2.04	.044	.205	.040	41.6	44.7	47.1	2.38	13.1	37.8	34.5
GP-9	2.57	.051	.186	.036	44.1	47.5	50.8	3.30	15.5	40.0	37.2
GP-10	3.00	.056	.172	.040	47.7	51.7	55.9	4.15	18.0	43.1	40.1
GP-11	3.02	.057	.173	.040	47.8	51.8	56.0	4.18	18.3	43.1	40.1
GP-12	3.30	.061	.182	.046	48.3	52.5	56.9	4.33	16.9	43.6	40.3
GP-13	3.35	.062	.186	.045	47.4	51.7	56.0	4.29	16.1	42.9	40.2
GP-14	3.10	.058	.187	.044	46.7	50.6	54.6	3.98	15.6	42.4	39.5
GP-15	3.15	.061	.192	.044	45.9	49.9	53.8	3.94	15.7	41.4	38.4
GP-16	2.61	.052	.205	.043	43.8	47.3	50.4	3.04	13.7	39.9	37.0
GP-17	2.53	.052	.215	.040	43.0	46.3	49.1	2.81	14.0	39.2	36.6
GP-18	2.18	.046	.224	.039	41.1	44.2	46.5	2.33	12.9	37.4	34.8
GP-19	2.21	.049	.233	.034	40.7	43.7	46.0	2.26	12.5	37.2	35.2
GP-20	1.72	.039	.243	.034	39.8	42.7	44.4	1.70	11.8	36.4	33.9
GP-21	.844	.023	.280	.042	24.2	25.3	25.7	.464	2.23	21.9	20.7
GP-22	1.79	.043	.261	.036	37.9	40.4	42.1	1.64	10.1	34.5	32.2
GP-23	1.72	.042	.271	.037	37.1	39.6	41.1	1.52	9.55	33.9	31.8
GP-24	.804	.025	.294	.046	28.2	30.7	31.3	.653	4.01	26.7	24.6
GP-25	.939	.031	.299	.045	28.4	29.9	30.7	.751	3.84	26.0	24.5
GP-26	.883	.032	.289	.042	26.9	28.4	29.1	.729	3.38	24.6	23.5
GP-27	1.11	.032	.252	.040	32.3	34.6	35.6	1.05	6.17	29.6	27.4
GP-28	.469	.019	.271	.039	25.5	26.7	27.1	.414	3.13	23.6	21.9
GP-29	.784	.028	.266	.037	27.5	29.0	29.7	.704	4.02	25.2	23.3
GP-30	.394	.016	.275	.051	24.1	25.2	25.5	.342	2.06	22.6	20.6
GP-31	.649	.023	.266	.049	27.0	28.6	29.1	.583	3.21	24.7	22.6
GP-32	.607	.023	.271	.050	26.3	27.5	28.1	.536	2.83	23.5	21.7
GP-33	.936	.030	.264	.050	28.4	29.7	30.6	.849	3.50	25.9	24.7
GP-34	.497	.018	.271	.048	25.9	27.1	27.5	.438	2.68	24.1	22.2
GP-35	.881	.032	.271	.046	27.1	28.5	29.3	.778	3.30	24.4	22.6
GP-36	.945	.033	.266	.043	27.9	29.3	30.1	.849	3.80	25.7	23.6
GP-37	.572	.023	.280	.041	24.9	26.0	26.5	.488	2.66	23.3	22.2

Table A.4 Steady-state heat transfer results for tests on a tube bundle with grid spacers.

Set	Q (W)	$\overline{Nu}$	Re	RxA_f^2	Pr	Gr_m (x10^4)	Gr_{T_D} (x10^3)	Gr (x10^4)	Tdrive °C
GC-1	586.	3.57	93.7	78.7	6.00	4.56	3.18	1.81	.537
GC-2	673.	5.13	102.	78.8	5.81	5.52	3.82	1.71	.610
GC-3	950.	6.27	141.	50.4	5.66	8.14	4.64	1.99	.707
GC-4	963.	6.92	139.	64.5	5.43	8.85	5.76	2.05	.815
GC-5	1088.	6.76	154.	52.5	5.37	10.3	5.77	2.31	.789
GC-6	1409.	8.29	196.	31.5	5.16	14.1	5.63	2.58	.727
GC-7	1537.	9.34	206.	39.3	4.98	16.3	7.68	2.73	.931
GC-8	1556.	9.56	205.	46.3	4.81	17.5	8.99	2.89	1.02
GC-9	2058.	10.9	265.	34.7	4.45	26.5	11.2	3.79	1.11
GC-10	2295.	10.9	283.	34.9	4.43	29.8	12.9	4.17	1.27
GC-11	1884.	8.54	252.	35.5	4.26	26.1	10.4	4.61	.955
GC-12	1963.	10.1	263.	46.2	3.99	30.3	14.7	4.60	1.20
GC-13	2024.	8.72	263.	58.9	3.78	34.4	18.9	6.04	1.40
GC-14	2211.	9.30	286.	44.6	3.71	38.8	16.8	6.38	1.20
GC-15	2314.	8.95	302.	45.7	3.57	43.3	19.2	7.32	1.28
GC-16	2123.	8.64	279.	60.0	3.69	37.6	21.5	6.59	1.52
GC-17	2071.	10.3	271.	57.2	3.89	33.5	19.4	5.05	1.51
GC-18	2057.	9.53	273.	37.4	4.06	30.9	12.8	4.90	1.08
GC-19	2097.	10.8	275.	45.6	4.04	31.8	15.8	4.55	1.32
GC-20	1923.	9.46	258.	36.2	4.18	27.5	11.1	4.52	.990
GC-21	2238.	11.4	295.	22.0	4.40	29.3	8.83	3.98	.861
GC-22	1857.	11.4	255.	23.7	5.23	18.1	7.16	2.47	.947
GC-23	1893.	11.9	258.	25.5	4.98	20.1	7.87	2.64	.955
GC-24	834.	7.26	124.	64.9	5.58	7.31	4.59	1.66	.683
GC-25	667.	4.68	103.	81.2	5.65	5.71	4.00	1.97	.608
GC-26	692.	5.67	110.	55.8	5.91	5.52	3.12	1.57	.513
GC-27	382.	4.13	61.9	164.	5.98	2.98	2.91	1.26	.489
GC-28	657.	4.31	107.	58.0	6.07	5.00	3.11	1.70	.537
GC-29	488.	3.54	84.7	81.7	6.25	3.54	2.70	2.08	.490
GC-30	402.	4.10	67.7	119.	6.11	3.04	2.52	1.29	.440
GC-31	449.	3.61	77.0	125.	6.19	3.31	3.43	1.48	.612
GC-32	305.	3.75	55.3	211.	6.40	2.13	2.98	1.02	.564
GC-33	542.	4.14	98.0	44.2	6.38	3.81	1.95	1.36	.368
GC-34	770.	4.50	132.	37.9	6.03	5.93	3.08	1.89	.524

Table A.4 (Continued)

GP-1	963.	7.98	139.	99.1	5.54	8.56	8.84	1.61	1.29
GP-2	1222.	7.60	190.	27.5	5.45	11.1	4.60	2.12	.657
GP-3	1253.	8.12	193.	29.8	5.23	12.2	5.12	2.28	.678
GP-4	1489.	9.38	224.	19.0	5.08	15.3	4.42	2.46	.555
GP-5	1588.	9.89	234.	33.9	4.91	17.3	8.59	2.67	1.01
GP-6	1668.	8.83	250.	22.6	4.76	19.1	6.55	3.24	.732
GP-7	2013.	11.3	299.	22.6	4.51	25.3	9.33	3.42	.949
GP-8	2043.	10.2	298.	24.5	4.37	27.1	10.1	3.99	.968
GP-9	2578.	12.2	369.	19.2	4.13	37.7	12.1	4.64	1.04
GP-10	3003.	12.4	430.	17.4	3.82	50.2	14.9	6.08	1.12
GP-11	3020.	12.2	436.	17.9	3.81	50.6	15.7	6.20	1.18
GP-12	3302.	13.0	473.	14.6	3.77	56.4	15.1	6.42	1.11
GP-13	3356.	13.8	475.	14.9	3.84	55.5	15.6	5.98	1.18
GP-14	3108.	13.9	441.	16.3	3.89	50.2	14.6	5.47	1.14
GP-15	3153.	13.3	454.	17.9	3.97	49.2	17.0	5.56	1.37
GP-16	2616.	12.7	372.	19.9	4.15	37.9	12.7	4.48	1.11
GP-17	2530.	12.7	363.	18.0	4.23	35.5	10.9	4.18	.994
GP-18	2187.	11.5	311.	22.2	4.42	28.5	9.94	3.71	.973
GP-19	2211.	11.9	324.	20.3	4.44	28.5	9.82	3.56	.972
GP-20	1728.	9.81	255.	30.7	4.54	21.5	9.24	3.31	.950
GP-21	544.	4.23	109.	26.9	6.58	3.63	1.48	1.16	.295
GP-22	1791.	9.98	274.	21.1	4.75	20.5	7.33	3.05	.819
GP-23	1724.	10.7	265.	21.6	4.84	19.2	7.01	2.72	.808
GP-24	804.	5.97	131.	44.9	5.83	6.56	3.59	1.52	.576
GP-25	939.	7.49	160.	27.3	5.94	7.42	3.24	1.47	.538
GP-26	883.	7.73	157.	25.4	6.16	6.58	2.91	1.28	.515
GP-27	1114.	7.88	176.	36.8	5.41	10.3	5.27	1.97	.742
GP-28	469.	5.37	89.8	31.9	6.33	3.33	1.18	1.01	.220
GP-29	784.	7.05	139.	35.9	6.06	5.99	3.20	1.32	.551
GP-30	394.	5.67	79.1	78.5	6.53	2.66	2.26	0.79	.443
GP-31	649.	5.85	114.	48.7	6.14	4.86	2.92	1.29	.514
GP-32	607.	4.05	110.	36.5	6.28	4.37	2.07	1.51	.379
GP-33	936.	7.90	157.	27.7	5.94	7.39	3.17	1.51	.526
GP-34	497.	5.90	89.6	45.5	6.27	3.59	1.68	.965	.307
GP-35	881.	6.26	158.	23.2	6.15	6.56	2.70	1.49	.477
GP-36	945.	8.31	167.	25.1	5.99	7.36	3.27	1.13	.551

NRC FORM 335 (2-84) NRCM 1102, 3201, 3202

U.S. NUCLEAR REGULATORY COMMISSION

BIBLIOGRAPHIC DATA SHEET

SEE INSTRUCTIONS ON THE REVERSE

1. REPORT NUMBER (Assigned by TIDC, add Vol. No., if any)

NUREG/CR-4556

2. TITLE AND SUBTITLE

Heat Transfer From A Rod Bundle Under Natural Circulation Conditions

3. LEAVE BLANK

4. DATE REPORT COMPLETED

MONTH	YEAR
December	1985

5. AUTHOR(S)

K.P. Hallinan, R. Viskanta

6. DATE REPORT ISSUED

MONTH	YEAR
March	1986

7. PERFORMING ORGANIZATION NAME AND MAILING ADDRESS (Include Zip Code)

Purdue University
Mechanical Engineering Building
West Lafayette, Indiana 47907

8. PROJECT/TASK/WORK UNIT NUMBER

9. FIN OR GRANT NUMBER

NRC-G-04-84-006

10. SPONSORING ORGANIZATION NAME AND MAILING ADDRESS (Include Zip Code)

Division of Accident Evaluation
Office of Nuclear Regulatory Research
U.S. Nuclear Regulatory Commission
Washington, DC 20555

11a. TYPE OF REPORT

Technical

b. PERIOD COVERED (Inclusive dates)

12/84-12/85

12. SUPPLEMENTARY NOTES

13. ABSTRACT (200 words or less)

Steady-state and transient experiments were performed in a rectangular natural circulation loop. Based on the steady-state data obtained, empirical correlations for fluid friction and heat transfer of the circulating fluid flowing through the tube bundle were developed. The pressure drop in the loop was found to depend on the Reynolds number. Friction factor relations for laminar forced flow through tube bundles were found to accurately model fluid friction of the circulating fluid through the test bundles. Empirical correlations for the average Nusselt number were developed for both parrallel-flow and counter-flow arrangements of the test bundle was found to have little effect on the total flow resistance of the circulating fluid, while enhancing the average heat transfer from 5% to 15%, depending on the thermal and flow conditions.

The dynamic response of the circulating fluid and of the loop structural components was predicted from a one-dimensional model. Good correspondence was obtained between the predicted and measured local temperatures and the time to reach steady-state conditions.

14. DOCUMENT ANALYSIS - a. KEYWORDS/DESCRIPTORS

Natural Circulation
Grahof Number
Reynolds Number
Fluid Friction
Form Loss Coefficient

b. IDENTIFIERS/OPEN ENDED TERMS

15. AVAILABILITY STATEMENT

Unlimited

16. SECURITY CLASSIFICATION

(This page) Unclassified

(This report) Unclassified

17. NUMBER OF PAGES

18. PRICE

UNITED STATES
NUCLEAR REGULATORY COMMISSION
WASHINGTON, D.C. 20555

120555078877 1 1AN1R4
US NRC
ADM-DIV OF TIDC
POLICY & PUB MGT BR-PDR NUREG
W-501
WASHINGTON DC 20555